SANDIA REPORT

SAND2005-0206
Unlimited Release
Printed January, 2005

ODTLES:
A Model for 3D Turbulent Flow Based on One-dimensional Turbulence Modeling Concepts

Rodney C. Schmidt
Randy McDermott
Alan R. Kerstein

Prepared by
Sandia National Laboratories
Albuquerque, New Mexico 87185 and Livermore, California 94550

Sandia is a multiprogram laboratory operated by Sandia Corporation,
a Lockheed Martin Company, for the United States Department of Energy's
National Nuclear Security Administration under Contract DE-AC04-94-AL85000.

Issued by Sandia National Laboratories, operated for the United States Department of Energy by Sandia Corporation.

Available to DOE and DOE contractors from
U.S. Department of Energy
Office of Scientific and Technical Information
P.O. Box 62
Oak Ridge, TN 37831

Telephone: (865) 576-8401
Facsimile: (865) 576-5728
E-Mail: reports@adonis.osti.gov
Online ordering: http://www.doe.gov/bridge

Available to the public from
U.S. Department of Commerce
National Technical Information Service
5285 Port Royal Rd
Springfield, VA 22161

Telephone: (800) 553-6847
Facsimile: (703) 605-6900
E-Mail: orders@ntis.fedworld.gov
Online ordering: http://www.ntis.gov/ordering.htm

SAND2005-0206
Unlimited Release
Printed January, 2005

ODTLES:
A Model for 3D Turbulent Flow Based on One-dimensional Turbulence Modeling Concepts

Rodney C. Schmidt
Computational Sciences Department
Sandia National Laboratories, P.O. Box 5800
Albuquerque, NM 87185-0316

Randy McDermott
Chemical Engineering Department, University of Utah
Salt Lake City, UT 84112

Alan R. Kerstein
Reacting Flow Research Department
Sandia National Laboratories, P.O. Box 0969
Livermore, CA 94551-0969

Abstract

This report describes an approach for extending the one-dimensional turbulence (ODT) model of Kerstein [6] to treat turbulent flow in three-dimensional (3D) domains. This model, here called ODTLES, can also be viewed as a new LES model. In ODTLES, 3D aspects of the flow are captured by embedding three, mutually orthogonal, one-dimensional ODT domain arrays within a coarser 3D mesh. The ODTLES model is obtained by developing a consistent approach for dynamically coupling the different ODT line sets to each other and to the large scale processes that are resolved on the 3D mesh. The model is implemented computationally and its performance is tested and evaluated by performing simulations of decaying isotropic turbulence, a standard turbulent flow benchmarking problem.

Acknowledgment

This work was primarily supported by the Laboratory Directed Research and Development (LDRD) program at Sandia National Laboratories. Special thanks to Dana Powers and Carl Peterson of the Sandia LDRD Seniors Council for their support of this work. In addition, we gratefully acknowledge the funding provided to R. McDermott through a Department of Energy Computational Science Graduate Fellowship (DE-FG02-97ER25308).

Contents

Appendix

Figures

Tables

ODTLES: A Model for 3D Turbulent Flow Based on One-dimensional Turbulence Modeling Concepts

1 Introduction

1.1 Modeling Turbulent Flow

Turbulent flow phenomenology is central to a remarkably wide range of engineering problems, including many, such as nuclear weapon physics, climate change, and commercial power conversion applications, that are relevant to key DOE missions. However, despite many years of intensive research, turbulence modeling remains a notoriously difficult problem. Cant [2] recently noted that computational fluid dynamics (CFD) is by far the largest user of high-performance computing in engineering, and argues that the premier scientific challenge confronting the fluids engineering community is to gain a greater understanding of turbulence and its consequences in engineering applications. Although it is tempting to hope that advances in computing speed and hardware will soon enable the direct numerical simulation (DNS) of such problems and thereby avoid the issue of modeling altogether, in reality, the extreme range of length and time scales associated with high-Reynolds-number flows will continue to limit the use of DNS (at least for the foreseeable future) to rather simple conditions at relatively low Reynolds numbers. Thus, turbulence models will continue to be indispensable tools in engineering analysis for many years to come.

The two most commonly used approaches for computationally modeling turbulent flow are (1) the Reynolds-averaged Navier-Stokes (RANS) approach, and (2) the large eddy simulation (LES) approach. The key difference between these models is that in RANS, the model equations are derived by ensemble or time averaging the governing Navier-Stokes equations, whereas in LES the model equations are obtained by a spatial filtering operation. In either case, special terms are introduced through the derivation process that must be represented with some additional closure model in order to solve the equations. Although RANS methods are widely used and are of great value in many engineering problems, experience over many decades has clearly demonstrated the inherent limitations of the approach, particularly as a predictive tool. Thus as computing power has increased, so also has interest in the LES approach.

In LES, the spatial filtering step masks motions smaller than a specified filtering length scale, but the large-scale three-dimensional unsteadiness not captured from RANS calculations is resolved. Although this leads to computational demands that are much larger than RANS, the cost can be worth it because the unsteadiness captured by LES is one of the most important features of many flows. The challenge introduced by eliminating the small scales is the need to model the non-linear 'subgrid scale' terms which represent the effects of unresolved physics on the resolved flow scales.

Unfortunately, the accurate modeling of these terms has proven particularly difficult for all but the simplest of flows. Long-standing efforts to develop an adequate closure, and the difficulties that have been encountered, are well documented (e.g. [9, 10]). Of particular note is a recent study that analyzed in detail the requirements for accurate closure for turbulent channel flow [14]. It was concluded that it is insufficient solely to capture the transfer of energy from grid-resolved to subgrid scales, and therefore that eddy-viscosity modeling, which addresses only this aspect of the interaction between grid-resolved and subgrid scales, is inadequate. At a minimum, the closure must also capture the subgrid transport (in particular, wall-normal transport in near-wall flow), subgrid stresses, and subgrid intercomponent transfer due to pressure effects. No traditional closure approach currently being pursued can demonstrably capture these effects in principle, let alone represent them accurately.

Another, more recently developed, turbulence model is the one-dimensional-turbulence (ODT) model of Kerstein [6, 7]. This model, and the concepts it has introduced, is at the core of the new approach developed here for LES.

ODT is a method for simulating the turbulent transport and dynamic fluctuations in velocity and fluid properties that one might measure along a one-dimensional (1D) line of sight through 3D turbulent flow. In contrast to RANS and LES, the ODT equations are not derived directly from the Navier-Stokes equations. In the 1D dynamical system defined by the ODT model, the effects of turbulent 3D eddies associated with real fluid flow are modeled by 1D fluid-element rearrangements, denoted eddy events, that occur over a range of length scales and with frequencies that depend on event length scales and instantaneous flow states. The first ODT formulation [6] involved simulation of a single velocity component evolving on a line. A more recent formulation [7] introduced the evolution of the three-component velocity vector on the 1D domain. Generalization to treat variable-density effects dynamically has also been demonstrated [1]. Because the model is 1D, well resolved calculations at high Reynolds numbers are affordable, and remarkably successful results have been demonstrated for a variety of canonical flows. However, this same 1D attribute has naturally limited its application to turbulence problems where spatial variations in only one direction are of primary interest.

Recently, ODT was successfully used as the basis for a near-wall subgrid closure model for LES [11, 12]. This application was natural because statistical variations in the near-wall region are primarily 1D. While developing the ODT-based LES near-wall model, a number of ideas were generated concerning how ODT and LES might be more generally combined. This report describes one such approach, although others may also be viable. The basic goal is for large-scale 3D turbulent motions to be captured by the LES part of the model and a representative sample of the small-scale turbulent motions to be simulated by the ODT part of the model. In this new approach, denoted ODTLES, revised ODT equations are formulated that allow physically realistic interaction between the ODT model of the small scales and the 3D LES representation of the large-scale motions.

Because ODTLES combines elements of both LES and ODT, a brief review of these modeling approaches is provided in the next two subsections.

1.2 A Synopsis of the LES Modeling Approach

The LES modeling approach is based on the concept of spatial filtering. Given any physical quantity $\phi(\mathbf{x},t)$ that is defined over some spatial domain $\mathbf{x}$, we can define a filtered quantity $\bar{\phi}(\mathbf{x},t)$ as

$$\bar{\phi}(\mathbf{x},t) = \int_D \phi(\mathbf{x},t) G(\mathbf{x}-\mathbf{z},\Delta)\, d\mathbf{z}, \tag{1}$$

where G is a normalized filter kernel, D is the domain of the flow, and Δ is the filter width. In LES, the shape and spatial extent of the filter applied is a modeling choice. For example, if the filter is defined as an anisotropic box filter, then the value of $\bar{\phi}(\mathbf{x},t)$ is simply the instantaneous average value of ϕ within the domain enclosed by a box centered around the point $\mathbf{x}$. Other filter types used in LES include the Gaussian filter and the sharp spectral filter.

The most common way to derive LES equations is to directly apply the concept of spatial filtering to the Navier-Stokes and continuity equations. For a filter that commutes with differentiation, and for an incompressible fluid with constant properties, one obtains

$$\rho \frac{\partial \bar{u}_i}{\partial t} + \rho \frac{\partial}{\partial x_j}(\overline{u_i u_j}) = -\frac{\partial \bar{p}}{\partial x_i} + \frac{\partial}{\partial x_j}\left[\mu\left(\frac{\partial \bar{u}_i}{\partial x_j}\right)\right] + \rho \bar{f}_i \tag{2}$$

$$\frac{\partial \bar{u}_i}{\partial x_i} = 0. \tag{3}$$

where f denotes a body force and repeated indices are used here to imply summation. The fields resolved on the LES mesh are $\bar{u}_i$ and $\bar{p}$, and the term $\overline{u_i u_j}$ must be modeled.

Although often thought of as the LES equations, no analytical solutions to these continuum forms of the LES equation for any problems of interest are known to the authors. All LES results are, in fact, solutions to some discrete numerical representation of Eqs. (2) and (3) (e.g., finite difference, finite volume, finite element, etc.) on a specified mesh, coupled with a particular closure model. Thus the real LES equations are always a discrete form of Eqs. (2) and (3) coupled with a particular closure model. This point may seem trivial, but is important for several reasons. First, all numerical methods introduce numerical error, an effect which in LES can be difficult to distinguish and separate from the effects of the subgrid models employed. Secondly, an alternative approach to developing LES equations, which has several advantages not discussed here, is to start directly from the finite-volume method just mentioned.

In the early LES literature Schumann [13] described and developed a discrete LES equation set based on the finite-volume numerical method. In this approach, called the 'volume-balance method,' the averaged quantities correspond to a discrete number of volumes that are fixed in space (i.e., the mesh). The governing equations are integrated by parts to obtain discrete budget equations

for the individual mesh cells. In this context the modeling problem is to represent accurately the unresolved surface fluxes in terms of the spatially averaged quantities that are available. Adopting Schumann's notation, the discrete LES equations that correspond to Eqs. (2) and (3) above can be written as

$$\rho\frac{\partial\overline{u_i}}{\partial t}+\rho\delta_j(\overline{u_iu_j}^S)=-\delta_i\overline{p}+\delta_j\left[\mu\left(\overline{\frac{\partial u_i}{\partial x_j}}^S\right)\right]+\rho\,\overline{f_i}, \tag{4}$$

$$\delta_j(\overline{u_i}^S)=0 \tag{5}$$

where δ denotes a numerical-difference operator, and the advective and diffusive flux terms (denoted by superscript S) are averages over surfaces, not volume averages.

No matter how the LES equations are derived, to solve them a closure model must be chosen for the nonlinear advective term (the second term in Eq. (2) or (4)). To this end, it is common to define a subgrid-scale stress tensor τ. This, we note, is NOT the approach adopted in ODTLES. However, for context it is useful to review this model because it is so commonly used. Reverting to the continuum form of the LES equations, we can write

$$\tau_{ij}=\overline{u_iu_j}-\overline{u}_i\overline{u}_j. \tag{6}$$

Gradient-diffusion models adopt the hypothesis that the anisotropic part of the subgrid-scale stress tensor τ is proportional to the resolved (large scale) strain-rate tensor $\mathbf{S}$:

$$\tau_{ij}-\frac{1}{3}\delta_{ij}\tau_{kk}=-2\frac{\mu_S}{\rho}\overline{\mathbf{S}}_{ij} \tag{7}$$

$$\overline{\mathbf{S}}_{ij}=\frac{1}{2}\left(\frac{\partial\overline{u}_i}{\partial x_j}+\frac{\partial\overline{u}_j}{\partial x_i}\right), \tag{8}$$

where μ_S is a subgrid eddy viscosity, which must be computed from an appropriate model, and δ_{ij} is the Kronecker delta. By defining a modified pressure $\overline{P}$ that includes the subgrid kinetic energy (i.e., the trace of τ), and dropping the body-force term $\rho\,\overline{f_i}$ for simplicity, Eq. (2) can now be expressed as

$$\rho\frac{\partial\overline{u}_i}{\partial t}+\rho\frac{\partial}{\partial x_j}(\overline{u}_i\overline{u}_j)=-\frac{\partial\overline{P}}{\partial x_i}+\frac{\partial}{\partial x_j}\left[(\mu+\mu_S)\left(\frac{\partial\overline{u}_i}{\partial x_j}\right)\right]. \tag{9}$$

One of the first models for the subgrid eddy viscosity was introduced by Smagorinsky and it remains, together with its variants, a widely applied model. It can be written compactly as

$$\mu_S=\rho(C_S\Delta)^2(2\overline{\mathbf{S}}_{ij}\overline{\mathbf{S}}_{ij})^{1/2}, \tag{10}$$

where C_S is called the Smagorinsky coefficient, and the characteristic filter width Δ is generally computed as the cube root of the local cell volume (e.g. see [4]):

$$\Delta = (\Delta x_1 \Delta x_2 \Delta x_3)^{1/3}. \tag{11}$$

1.3 One-Dimensional Turbulence Modeling (ODT)

We now turn our attention to the ODT modeling approach. Unlike LES or RANS, which are derived directly from the Navier-Stokes equations, ODT cannot be described solely with a set of continuum equations. Rather, the important physics affecting the 3D turbulent flow along a 1D line of sight are phenomenologically modeled. In ODT the fields defined on the 1D domain evolve by two mechanisms: (1) molecular diffusion, and (2) a sequence of instantaneous transformations, denoted 'eddy events,' which represent turbulent stirring. These eddy events occur over a large range of length scales, with frequencies that depend on event length scales and instantaneous flow states.

Between the occurrence of eddy events, the time evolution of ODT velocity components v_i on an ODT line in direction x can be written as

$$\frac{\partial v_i}{\partial t} - \nu \frac{\partial^2 v_i}{\partial x^2} = 0, \tag{12}$$

where t denotes time and ν is the kinematic viscosity.

The evolution of the velocity field defined by Eq. (12) is interrupted at various points in time by the previously mentioned eddy events. Each eddy event may be interpreted as the model analog of an individual turbulent eddy, and consists of up to two mathematical operations that can be represented symbolically as

$$v_i(x) \rightarrow v_i(f(x)) + c_i K(x). \tag{13}$$

According to this prescription, fluid at location $f(x)$ is moved to location x by the mapping operation, thus defining the map in terms of its inverse $f(x)$. In ODT we use a special measure-preserving map, called the 'triplet map,' which in any discrete implementation simply corresponds to an exchange of fluid elements according to a predefined pattern. The second operation indicated is an energy-conserving modification of the velocity profiles used to implement energy transfers among velocity components. This operation is only applicable when more than one velocity component is being modeled, and is used to model pressure-induced energy redistribution among velocity components.

The frequency of eddy events is governed by a probabilistic model that depends on the current instantaneous velocity field, the eddy location and its length scale. Details can be found in Kerstein

[6, 7], and will not be repeated here. Of note here is that ODT requires the specification of three model parameters. The most important of these is the overall rate constant, C, which controls the relative strength of the turbulent stirring model. The other two model parameters are the viscous cutoff parameter Z and the energy transfer coefficient α.

A key aspect of ODT is how eddy events modify 1D property/velocity profiles, thus modifying the spatial distribution of velocity and kinetic energy. The resulting two-way coupling between velocity profiles and the eddy rate distribution leads to complex behavior that emulates both the gross structure and the fine-grained intermittency of the 3D turbulent cascade. It is also noteworthy that the model completely avoids the use of eddy viscosity concepts to model transport or energy transfer.

2 Model Description

In this section we describe ODTLES, an approach for extending the one-dimensional turbulence model of Kerstein [6] to treat turbulent flow in three-dimensional domains. ODTLES can also be thought of as a novel LES approach, and we will show how large-scale 3D turbulent motions are captured by the LES aspects of the model but are strongly coupled to the small-scale turbulent motions generated by the ODT part of the model.

Before continuing we also note that ODT might be combined with LES in at least two different ways. One option is to start with the LES equations (derived by spatially averaging the NS equations), and seek a method for using ODT as a subgrid closure model for these equations. This can be thought of as a top-down approach, and is denoted LES/ODT. A second option is to begin with the ODT equations, and then add additional terms so that mutually orthogonal ODT domains might be coupled together and 3D LES modeling constraints enforced. The ODTLES model described here follows the latter bottom-up approach.

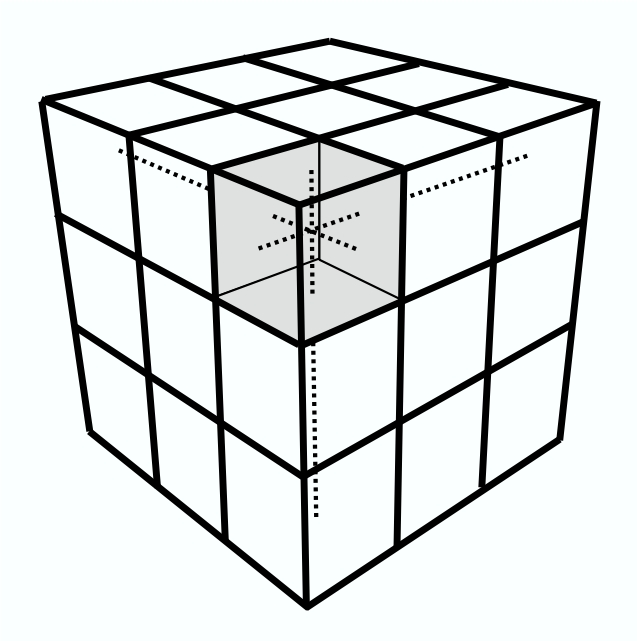

Figure 1. Illustrative geometry of the ODT and LES subdomains

2.1 Geometry and Numerical Discretization

In ODTLES we discretize our domain of interest in two distinct but interdependent ways. The first is by a standard set of rectangular control volumes. The second is formed by embedding three, mutually orthogonal ODT domain arrays within the coarser 3D mesh. This is illustrated in Figure 1 for a simple box-shaped region. Here we see that the overall domain is subdivided into N_{les}^3 uniform LES control volumes, where $N_{les} = 3$ is the number of LES-scale subdivisions in each

direction. A 2D array of N_{les}^2 ODT lines are also placed in each coordinate direction. This forms a network of lines that intersect each other at the center of each LES control volume, as illustrated in Figure 2. Note that only the three lines that intersect in the shaded control volume are shown in Figure 1. Overall there are $3N_{les}^2$ ODT lines that extend through the computational domain.

On each ODT line, N_{odt} mesh points are defined, where $N_{odt} > N_{les}$. The value of N_{odt} must be large enough so that the smallest scales of the turbulent motion are adequately resolved. (Later this constraint will be relaxed by the introduction of a subgrid model for ODT.) The total number of mesh points in the problem is therefore $3 * N_{les}^2 * N_{odt}$. This can be compared with the total number of points that would be required for a direct numerical simulation, which is $3 * N_{odt}^3$.

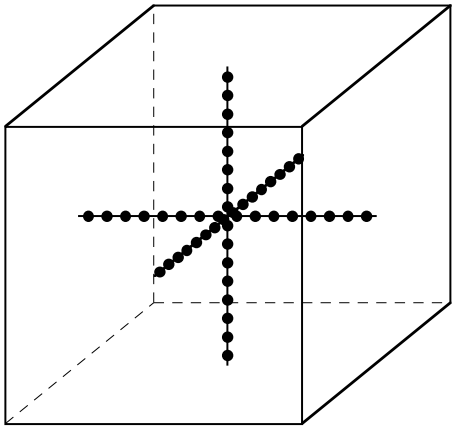

Figure 2. Three ODT lines intersect each LES control volume

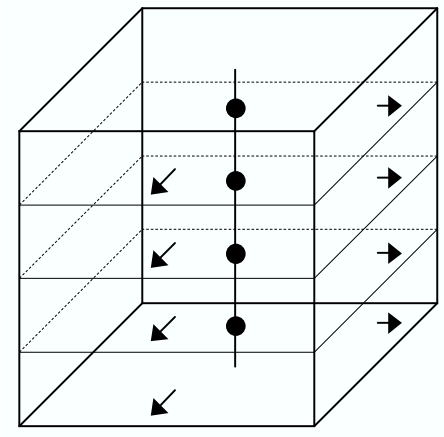

Figure 3. Staggered location of ODT velocity components

Associated with each ODT line direction k (k=1-3), we define two ODT velocity components, $v_{k,i}$ $(i \neq k)$, corresponding to the two coordinate directions that are orthogonal to the line. This two-component model is a simplification of the three-component vector formulation described in [7],

and is summarized below in Section 2.2. Although a 3-component ODT model would also work in the formulation presented here, the velocity component parallel to each ODT line would not be used in any direct way. Thus, for numerical efficiency reasons, we have adopted the 2-component model for the present purposes.

Although instantaneous ODT values are conceptualized as point values, a sub-control volume is also defined for the purpose of preserving certain conservation properties described later. As illustrated in Figure 3 for a vertical (k=2) ODT line, the staggered locations of the two velocity components are associated with the ODT sub-control volume faces in the standard way.

In ODTLES numerics, there are two important length scales, $\Delta x \ll \Delta X$, and two important time scales, $\Delta t \ll \Delta T$. These are, respectively, the ODT and LES spatial discretization lengths and the ODT and LES time steps.

2.2 A two-component formulation of ODT

The version of ODT utilized here describes the evolution of a two-component vector velocity field $v_i(x,t)$ defined on a 1D domain, parameterized by the spatial coordinate x, which is assumed orthogonal to the two velocity component directions. This formulation follows in all key respects the three-component vector formulation described in [7].

The fields defined on the 1D domain evolve by two mechanisms, molecular evolution and a stochastic process representing turbulent stirring. The stochastic process consists of a sequence of 'eddy events,' each of which involves an instantaneous transformation of the velocity and scalar fields. During the time intervals between eddy events, the molecular evolution of ODT velocity components is governed by Eq. (12).

The turbulent stirring submodel is specified by defining the mathematical operations performed during an eddy event and by formulating the rules that govern the selection of events. Because the model has multiple velocities, an eddy event consists of two mathematical operations. One is a measure-preserving map representing the fluid motions associated with a notional turbulent eddy. The other is a modification of the velocity profiles in order to implement energy transfers prescribed by the dynamical rules. These operations are represented symbolically by Eq. (13). According to this prescription, fluid at location $f(x)$ is moved to location x by the mapping operation, and the additive term $c_i K(x)$, is used to model pressure-induced energy redistributions among velocity components.

The functional form chosen for $f(x)$ is called the 'triplet map, and can be defined mathematically as

$$f(x) \equiv x_0 + \begin{cases} 3(x-x_0) & \text{if } x_0 \le x \le x_0 + \frac{1}{3}l, \\ 2l - 3(x-x_0) & \text{if } x_0 + \frac{1}{3}l \le x \le x_0 + \frac{2}{3}l, \\ 3(x-x_0) - 2l & \text{if } x_0 + \frac{2}{3}l \le x \le x_0 + l, \\ x - x_0 & \text{otherwise.} \end{cases} \tag{14}$$

This mapping takes a line segment $[x_0, x_0 + l]$, shrinks it to a third of its original length, and then places three copies on the original domain. The middle copy is reversed, which maintains the continuity of advected fields and introduces the rotational folding effect of turbulent eddy motion. Property fields outside the size-l segment are unaffected.

In Eq. (13), K is a kernel function that is defined as $K(x) = y - f(x)$, i.e., its value is equal to the distance the local fluid element is displaced. It is non-zero only within the eddy interval, and it integrates to zero so that energy redistribution does not change the total (y-integrated) momentum of individual velocity components. It provides a mechanism for energy redistribution among velocity components, an important characteristic that enables the model to simulate the tendency of turbulent eddies to drive the flow toward isotropy.

For an equipartition of available energy (see [7]), the values of c_i are governed by the relation

$$c_i = \frac{27}{4l}\left(-v_{i,K} + \mathrm{sgn}(v_{i,K})\sqrt{\frac{1}{2}(v_{i,K}^2 + v_{j,K}^2)}\right), \tag{15}$$

where the two velocity components are denoted by the subscripts i and j, and

$$v_{i,K} \equiv \frac{1}{l^2}\int v_i(f(x))K(x)\,\mathrm{d}x = \frac{4}{9l^2}\int_{x_0}^{x_0+l} v_i(x)[l - 2(x - x_0)]\,\mathrm{d}x. \tag{16}$$

The final ingredient required in the model is the determination of the time sequence of eddy events, individually parameterized by position x_0 and size l, that are implemented. In ODT, eddy events are implemented instantaneously, but must occur with frequencies comparable to the turnover frequencies of corresponding turbulent eddies. Events are therefore determined by sampling from an event-rate distribution that reflects the physics governing eddy turnovers. A key feature of this distribution is that it is based on the instantaneous state of the flow, and thus evolves in time as the flow evolves.

At each instant in time, the event-rate distribution is defined by first associating a time scale $\tau(y_0, l)$ with every possible eddy event. To this end, the quantity l/τ is interpreted as an eddy velocity and $\rho l^3/\tau^2$ is interpreted as a measure of the energy of eddy motion. To determine τ, this energy is equated to an appropriate measure of the eddy energy based on the current flow state. The energy measure used here is the current available energy in the two velocity components, minus an energy penalty that reflects viscous dissipation effects. (Note that this choice is slightly different than that used in [7].)

Based on these considerations, we write

$$\left(\frac{l}{\tau}\right)^2 \sim \left(v_{i,K}^2 + v_{j,K}^2 - Z\frac{\nu^2}{l^2}\right). \tag{17}$$

Given Eq. (17), the time scales τ for all possible eddies can be translated into an event-rate distribution λ, defined as

$$\lambda(x_0,l;t) \equiv \frac{C}{l^2\tau(x_0,l;t)} = \frac{C\nu}{l^4}\sqrt{\left(\frac{v_{i,K}l}{\nu}\right)^2+\left(\frac{v_{j,K}l}{\nu}\right)^2 - Z}, \tag{18}$$

where C is the ODT model parameter that controls the overall event frequency. If the argument of the square root is negative, the eddy is deemed to be suppressed by viscous damping and λ is taken to be zero for that eddy. In the square root term of Eq. (18), the quantities preceding Z involve groups that have the form of a Reynolds number. Z can be viewed in this context as a parameter controlling the threshold Reynolds number for eddy turnover.

An stand-alone applications, the maximum length L_{max} is constrained by the boundary conditions. However, in ODTLES, L_{max} is conceptualized as being linked to the size of the smallest 3D eddies resolvable by the LES mesh. For this reason its specification becomes part of the model.

2.2.1 Ensemble Mean Closure (EMC) of unresolved ODT

Just as a numerical DNS must fully resolve all 3D length and time scales in order to be valid, so must the ODT model fully resolve all 1D length and time scales. For high-Reynolds-number flows this resolution requirement dictates very refined grids that, even in only 1D, are computationally expensive. Recently, McDermott et al. [8] developed a gradient-diffusion based LES closure model which, in form, resembles a Smagorinsky-type eddy viscosity model, but which is derived entirely from ODT. Called ensemble mean closure (EMC), this approach was born of a desire to better understand ODT and to provide a theoretical basis for the empirically observed rate constant for LES/ODT in isotropic turbulence simulations. The resulting model is a legitimate LES subgrid model on its own, and eliminates the laminar flow finite-eddy-viscosity problem which plagues the constant-coefficient Smagorinsky model. Here, we employ EMC as a subgrid model for ODT. This is very useful in the context of the ODTLES model as it removes the requirement that the ODT mesh resolve the flow to the Kolmogorov scale. Later we will show that for high-Reynolds-number flows this results in considerable costs savings while giving the analyst almost complete freedom to choose the degree to which the sub-LES-grid scales are resolved by ODT in the simulation.

The EMC subgrid -tress closure is based on the mappings and time-scale physics employed in ODT. A simplified ODT model is envisioned in which eddy events only act upon the LES-resolved velocity field and stresses are based on ensemble averaged momentum transport by ODT eddy events, rather than the usual stochastic eddy sampling. As mentioned, the resulting model is analogous to conventional gradient-diffusion based LES closures such as the constant-coefficient Smagorinsky model.

The form of the ensemble closure (which is independent of the linearization) is obtained by accounting for all eddy events which can affect a given location, x, on an ODT line. First, we find the amount of momentum displaced across x, for an eddy parameterized by its starting location,

x_o, and length scale, l. The amount of momentum displaced, $\psi(x;x_o,l)$, is then multiplied by the event-rate density of the eddy, given by $1/l^2\tau$, where τ is the eddy time scale. With this, the form of the stress can be written as

$$R(x) = \int_{l_{min}}^{l_{max}} \int_{x-l}^{x} \frac{\psi(x;x_o,l)}{l^2\tau} dx_o dl. \tag{19}$$

The integration limits reflect the range of x_o and l space which can possibly affect x. The maximum and minimum eddy lengths to be represented by the EMC model are denoted l_{max} and l_{min}. Completion of the model requires specification of the displacement function ψ and the eddy time scale τ, which are functions of the particular ODT model employed. This can be directly applied to calculate an ODT-based subgrid eddy viscosity whose form is analogous to Eq. (10).

Neglecting the small viscous cut-off effect (typically negligible for high Reynolds numbers), the EMC-based ODT subgrid eddy viscosity for the 2-component ODT model used here is written as

$$\mu_S = \rho C C_{emc} (l_{max})^2 \left(\left| \frac{\partial v_i}{\partial x_k} \right| + \left| \frac{\partial v_j}{\partial x_k} \right| \right) \tag{20}$$

where C is the ODT eddy rate constant, C_{emc} is an EMC model coefficient, and l_{max} is the largest eddy length NOT resolved by the ODT discretization. We note that Eq. 20 is slightly different than the analogous equation tested in [8], and thus the values of the model coefficients are not expected to be the same.

Based on the triplet map, the smallest eddy size that can be resolved by ODT is always $6\Delta x$. Thus l_{max} is always known from the ODT grid size.

If we include the EMC model, the evolution equation for 2-component stand-alone ODT can now be written as

$$\frac{\partial v_i}{\partial t} - \frac{\partial}{\partial x} \left((\nu + \nu_S) \frac{\partial v_i}{\partial x} \right) = 0 \tag{21}$$

where $\nu_S = \mu_S/\rho$, and ν_S is given by Eq. 20.

2.3 The ODTLES Evolution Equations

In ODTLES, local 3D coupling among the different velocity components is captured by adding several additional terms to the right-hand-side (RHS) of the stand-alone ODT equation, Eq. (21). Global 3D coupling is achieved by defining an LES-scale pressure field that is resolved on the 3D mesh and by requiring a 3D continuity equation to be satisfied.

The ODTLES evolution equations on each line in direction k (k=1-3) that will be solved for the individual ODT velocity components i ($i \neq k$) can be written conceptually as:

$$\frac{\partial v_{k,i}}{\partial t} - \frac{\partial}{\partial x_k}\left((\nu + \nu_{S,k})\frac{\partial v_{k,i}}{\partial x_k}\right) = -(LES\_Pres.)_i - (LES\_Conv.)_{k,i} + (3D\_Visc.)_{k,i}. \tag{22}$$

Here, as in all equations to follow (unless specifically noted), repeated indices are NOT used to imply summation.

In contrast to the stand-alone ODT model, where the RHS is zero, this revised equation has three additional terms. These terms will be used to model the LES-scale pressure-gradient, LES-scale convection, and multi-dimensional viscous effects on the evolution of the ODT velocity components.

Before describing a model for each of these additional terms, we define a set of quantities used in the model formulation.

Definitions

$\frac{\delta}{\delta x}$ Numerical difference operator acting on the LES scale

$\frac{\partial}{\partial x}$ Numerical difference operator acting on the ODT scale

$\bar{P}$ LES-scale pressure associated with each 3D control volume. Pressure is not defined on the individual ODT lines.

T A time scale which should be of order the eddy turnover time for the smallest 3D eddies resolved on the 3D mesh. In all calculations performed here, T is set equal to the LES time step, ΔT

ΔX The width of a 3D control volume.

$\bar{u}_{k,i}$ A time average of $v_{k,i}$ ($i \neq k$) over time-scale T, where

$$\bar{u}_{k,i} = \frac{1}{T}\int_{t-T}^{t} v_{k,i}\,dt. \tag{23}$$

$\bar{u}_{k,k}$ A time-averaged velocity parallel to ODT line k that is computed by requiring a $\bar{u}_{k,i}$-based continuity equation to be satisfied in each ODT sub-control volume associated with the ODT points on line k. These sub-control volumes and the spatial locations of other ODT velocities are illustrated in Figure 4.

$$\bar{u}_{k,k}(x_k) = \bar{u}_{k,k}(0) - \int_0^{x_k} \left(\frac{\delta \bar{u}_{k,i}}{\delta x_i} + \frac{\delta \bar{u}_{k,j}}{\delta x_j} \right) dx_k \tag{24}$$

where i, j, k is any permutation of the indices (1,2,3).

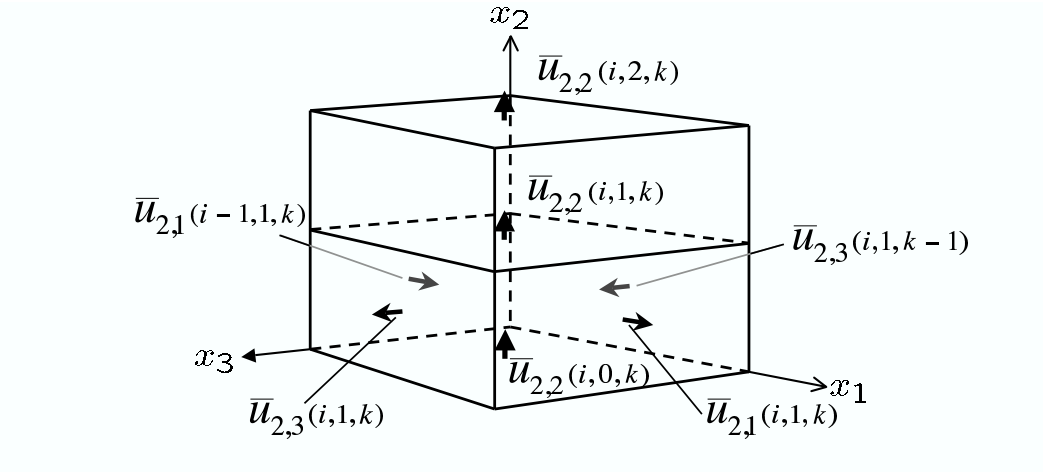

Figure 4. Orientation of $\bar{u}_{k,k}$ relative to $\bar{u}_{k,i}$ for a k=2 line.

$\bar{U}_i$ A spatial average over a control volume of the time-averaged velocity component $\bar{u}_{k,i}$.

$$\bar{U}_i = \frac{0.5}{\Delta X_k} \int_{\frac{-\Delta X_k}{2}}^{\frac{+\Delta X_k}{2}} \bar{u}_{k,i} dx_k + \frac{0.5}{\Delta X_l} \int_{\frac{-\Delta X_l}{2}}^{\frac{+\Delta X_l}{2}} \bar{u}_{l,i} dx_l \tag{25}$$

where i, k, l is any permutation of the indices (1,2,3).

Hereafter we refer to this temporally and spatially filtered velocity as the "LES" velocity field. It's location, consistent with the location of the $\bar{u}_{k,i}$ odt velocities, is geometrically located on control volume faces as per a standard staggered-grid scheme.

2.3.1 3D continuity and the LES-scale pressure-gradient term

Conservation of mass is enforced in the 3D domain by requiring the LES velocity field to satisfy the following discrete continuity equation on the LES grid:

$$\frac{\delta \bar{U}_1}{\delta x_1} + \frac{\delta \bar{U}_2}{\delta x_2} + \frac{\delta \bar{U}_3}{\delta x_3} = 0 \tag{26}$$

where $\bar{U}_i$ is defined in terms of the ODT velocity components as described above. This LES-scale continuity equation is enforced indirectly through the pressure field. The pressure field couples to the velocity field through a pressure gradient term in the evolution equations for the ODT velocity components (i.e., the momentum conservation equations). In ODTLES, the LES-scale pressure gradient term is modeled as:

$$(LES\_Pres.)_i = \frac{\delta \bar{P}}{\delta x_i}. \tag{27}$$

2.3.2 LES-scale convection term

The purpose of the LES-scale convection term is to model the 3D transport of momentum due to the resolved velocity field. This transport is distinct from that due to eddy events, whose purpose is to model the unresolved turbulent stirring.

In the current model, the LES-scale convection term is

$$(LES\_Conv.)_{k,i} = -\frac{\delta}{\delta x_i}(\bar{u}_{k,i}v_{k,i}) - \frac{\delta}{\delta x_j}(\bar{u}_{k,j}v_{k,i}) - \frac{\partial}{\partial x_k}(\bar{u}_{k,k}v_{k,i}) \tag{28}$$

where the time-averaged velocity field is used for the advecting velocities, as in [11]

2.3.3 Multi-dimensional viscous term

Diffusional transport parallel to the ODT line is modeled by the fully resolved viscous term that appears as the second term on the LHS of Eq. (22). The purpose of introducing an additional viscous term is to model diffusional transport of momentum in the two coordinate directions orthogonal to the ODT line. In addition, this model will contribute to the local energy dissipation rate due to viscous effects. For any line parallel to the k coordinate (hereafter denoted a k line), the two directions that must be accounted for are the longitudinal direction (to be denoted here with the subscript i) and the transverse direction (to be denoted with the subscript j). Because velocity gradients are not locally resolved in these two directions, we seek the best available information to approximate the required terms.

To model the transverse direction, we leverage the fact that i-component velocity gradients in the j-direction are fully resolved on all j-direction lines, and these lines intersect a k-line every ΔX. Therefore, we can model the transverse term at any point on line k by interpolation from the nearest two j-line intersection points. This approximation is convenient, consistent with the concept that ODT values are point values, and means that the velocity gradients felt by the ODT points on line k will have the proper magnitude and statistical variation. However, a small momentum-conservation error is also introduced by this approximation because the sum of all momentum fluxes to/from all ODT points is no longer balanced by construction. This error could be corrected

with the introduction of a supplementary LES-scale momentum-balance equation, but was not deemed necessary for the present work as the error introduced is small, symmetric around zero, and tends to zero with time averaging.

Because we have chosen to use a two-component ODT model (those being the two components orthogonal to the line-direction), resolved velocity gradients in the longitudinal direction are not available at intersection points. Therefore, gradients in this direction must be found using finite differences on the LES scale. Although we expect the overall the error introduced by this approximation to be small in most cases, alternative ways to account for this term are being looked at. For example, if a three-component ODT model were being used, then interpolation from the nearest two k-line intersection points (analogous to how the transverse term is treated) would be possible.

Given the modeling choices just described, the additional viscous transport term for each of the two velocity components $v_{k,i}$ defined on ODT line k, can be written as

$$(3D\_Visc.)_{k,i} = \frac{\partial}{\partial x_j}\left((\nu+\nu_{S,j})\frac{\partial v_{j,i}}{\partial x_j}\right)|_{jk-interp} + \frac{\delta}{\delta x_i}(\nu\frac{\delta v_{k,i}}{\delta x_i}) \tag{29}$$

where the suffix $|_{jk-interp}$ denotes evaluation by interpolation between values located at j-k line-intersection points.

2.3.4 Summary of the ODTLES Evolution Equations

The complete equation set describing the evolution of the ODTLES velocity components $v_{k,i}$ between eddy events can now be written. In these equations k denotes an ODT line in coordinate direction k, and the indices i, j, k are any permutation of the indices (1,2,3).

$$\begin{aligned}\frac{\partial v_{k,i}}{\partial t} - \frac{\partial}{\partial x_k}\left((\nu+\nu_{S,k})\frac{\partial v_{k,i}}{\partial x_k}\right) = \quad & -\frac{\delta \bar{P}}{\delta x_i} \\ & -\frac{\delta}{\delta x_i}(\bar{u}_{k,i}v_{k,i}) - \frac{\delta}{\delta x_j}(\bar{u}_{k,j}v_{k,i}) - \frac{\partial}{\partial x_k}(\bar{u}_{k,k}v_{k,i}) \\ & +\frac{\partial}{\partial x_j}((\nu+\nu_{S,j})\frac{\partial v_{j,i}}{\partial x_j})|_{jk-interp} + \frac{\delta}{\delta x_i}(\nu\frac{\delta v_{k,i}}{\delta x_i})\end{aligned} \tag{30}$$

subject to the 3D continuity constraint that

$$\frac{\delta \bar{U}_1}{\delta x_1} + \frac{\delta \bar{U}_2}{\delta x_2} + \frac{\delta \bar{U}_3}{\delta x_3} = 0 \tag{31}$$

where $\bar{u}_{k,i}$ and $\bar{U}_i$ are defined in terms of the ODT velocity components $v_{k,i}$ by Eqs. (23) and (25):

At this point it is instructive to consider certain limiting cases of the LESODT evolution equations.

First consider the limiting case in which the length scales ΔX_k and time scale T go to zero. Here ODT is viewed in the space-time continuum, and no eddy events occur because all motion is resolved in 3D. In this case $v_{k,i} = \bar{u}_{k,i} = \bar{U}_i$. Therefore Eq. (30) reduces to two identical copies of the incompressible form of the Navier-Stokes equations, and Eq. (31) reduces to the standard incompressible continuity equation.

Next consider the opposite case where the length scales ΔX_k and time scale T go to infinity. Under these conditions all of the LES scale convective and viscous transport terms on the RHS of Eq. (30) either become constant or go to zero, and Eq. (31) becomes meaningless. What remains are a set of 1D equations that are the evolution equations for a stand-alone ODT model.

2.3.5 Numerical Procedure

To begin a calculation, initial values for $v_{k,i}$ and $\bar{u}_{k,i}$ must be specified on all ODT lines subject to the constraint that the LES-scale continuity equation is satisfied. The LES pressure field $\bar{P}$ is also initialized to zero.

The ODTLES equations are integrated from LES time-step n to n+1, through the following sequence of steps.

(1) Evolve the ODT equations in time (using the ODT time-step Δt) on each individual ODT line over a time period equal to the LES time step.

Remark: The numerical implementation of an ODT simulation involves three subprocesses: molecular evolution, eddy selection, and eddy implementation. In the calculations performed here Eq. (22) is time-advanced each time the eddy event-rate distribution is sampled, leading to very small ODT time steps. Therefore first-order explicit time integration coupled with second-order central differencing of all other terms is employed. The procedure for eddy selection and eddy implementation is described in [7] (also see [11, 12]).

(2) Compute the intermediate values of $\tilde{\bar{u}}_{k,i}^{n+1}$ and $\tilde{\bar{U}}_{k,i}^{n+1}$ from the definitions given in Eqs. (23) and (25). The hat is used here to denote the intermediate nature of these values.

(3) For each ODT line compute ODT resolved values for a smooth continuous function $f(\tilde{\bar{U}}_{k,i}^{n+1})_{k,i}$ whose cell average matches the LES cell average values, Eq. (25). An efficient procedure for doing this is described in Appendix A. Then, on each line and at each ODT point location, compute and store the following difference quantities,

$$v'_{k,i} = v_{k,i} - \tilde{\bar{u}}_{k,i}^{n+1} \tag{32}$$

and

$$\vec{u}'_{k,i} = \tilde{\hat{u}}^{n+1}_{k,i} - f(\tilde{\hat{U}}^{n+1}_i)_{k,i}. \tag{33}$$

Remark: These differences will be used to reconstruct the ODT velocity fields after the LES velocity field has been adjusted to a divergence-free state through a pressure-projection step.

(4) Solve the following discrete Poisson equation for the pressure correction ϕ.

$$\frac{\delta^2\phi}{\delta x_i \delta x_i} = \left(\frac{1}{\Delta T}\right)\frac{\delta \tilde{\hat{U}}^{n+1}_i}{\delta x_i} \tag{34}$$

where the repeated indices are used in this equation to imply summation in the standard way.

(5) Compute the LES pressure and velocity fields at time n+1 via the following pressure and velocity correction equations.

$$\bar{P}^{n+1} = \bar{P}^n + \phi, \tag{35}$$

$$\bar{U}^{n+1}_i = \tilde{\hat{U}}^{n+1}_i - \Delta T\left(\frac{\delta\phi}{\delta x_i}\right), \tag{36}$$

Remark: Steps 4 and 5 correspond to a standard projection step that enforces the LES continuity constraint, Eq. (31).

(6) Compute the corrected values of $\bar{u}_{k,i}$ and $v_{k,i}$ based on the ODT reconstruction equations

$$\bar{u}^{n+1}_{k,i} = f(\bar{U}^{n+1}_i)_{k,i} + \vec{u}'_{k,i} \tag{37}$$

and

$$v_{k,i} = \bar{u}^{n+1}_{k,i} + v'_{k,i}. \tag{38}$$

Remark: The adjusted values of $v_{k,i}$ and $\bar{u}_{k,i}$ are now consistent with the new pressure-projected LES velocity field. This reconstruction procedure is designed so that high-wave-number (i.e. small-scale) fluctuations resolved at the ODT level are relatively unaffected by this procedure.

(6) Compute the values of $\bar{u}_{k,k}$ per Eq. (24).

This completes the LES time-step cycle.

2.3.6 Implicit LES momentum equation

So far, we have described ODTLES primarily from the ODT perspective. However, it can also be cast in the form of a volume-balance LES model as described by Schumann. In the volume-balance LES method the averaged quantities correspond to a discrete set of control volumes that are fixed in space. Here we extend this concept into the temporal domain by viewing the LES quantities as also time-averaged over a time scale T, where T is of order the LES time step ΔT. Thus in ODTLES, the $\bar{U}_i$ velocities can be properly viewed as LES quantities.

Because $\bar{U}_i$ are defined in terms of the $v_{k,i}$, a separate LES-scale momentum equation is not directly solved. However, by construction an LES-scale momentum equation is implicitly being satisfied by the formulation. This equation can be found by properly summing the individual contributions made by each ODT velocity equation to the change in $\bar{U}_i$ over a discrete LES time step. These changes are due to four processes: LES-scale pressure gradients, viscous diffusion across control volume surfaces, LES-scale advective transport across control volume surfaces, and momentum transport due to eddy events whose range extends across control volume surfaces. The first three of these processes occur continuously in time and are associated with the ODT evolution equation, Eq. (30). They can therefore be properly expressed as rates. In contrast, eddy events happen at random epochs, and their effect must be represented through a summation.

3 Simulations of Decaying Isotropic Turbulent Flow

For many years the simulation of decaying isotropic turbulent flow has served as an important but relatively simple test problem for turbulence models, theories, and computer codes. It is an excellent first test because the problem is posed in a fully periodic domain and complications that arise near solid walls are avoided. Although the idealized conditions are cast as a stationary problem that is for practical purposes unachievable in an experiment, space-time correlation measurements from the nearly isotropic turbulent flow downstream of a regular grid provide an excellent approximation. This is because Taylor's hypothesis can be used to show that spatially decaying grid turbulence is analogous to temporally decaying turbulence in a spatially fixed region. Important data sets include the classic experiment by Comte-Bellot and Corrsin [3] (hereafter referred to as CBC) and the more recent work of Kang, Chester and Meneveau [5] (to be denoted KCM). The CBC data is very well known and has been used in a large number of LES studies. However, the Reynolds number is quite low ($Re_\lambda = 72$). The more recent experiment of KCM was specifically designed as an update to the CBC results based on turbulence at a higher Reynolds number ($Re_\lambda = 720$) and includes detailed measurements that are of particular interest to the LES community.

In this section we compare ODTLES simulations with the KCM experimental data.

3.1 Geometry and Initial Conditions

The LES domain is a cube with edge length $L_{box} = 2\pi$. The 3D Cartesian mesh has an equal mesh spacing $\Delta X = L_{box}/N_{les}$ in all three directions. Most calculations are performed on a relatively coarse LES mesh size of $N_{les}^3 = 32^3$, but a comparison is also made with $N_{les}^3 = 64^3$. The ODT mesh size is varied from N_{odt} = 128 to 1024 to illustrate the impact of ODT mesh resolution on results and cost. The initial condition for the LES velocity field is generated by superimposing Fourier modes with random phases to match the initial 3D energy spectrum of the experimental data. Periodic boundary conditions are applied in all three directions. To develop coherent turbulent structure in the initial field, the random modes are allowed to evolve for a short time (several time steps), during which time the energy decays. Energy is then injected back into the Fourier modes such that the spectrum of the initial condition again matches the spectrum of the initial experimental data. This process is repeated several times until the coherent structures stabilize.

Without DNS data, the initialization of the ODT field is problematic. The procedure followed here is as follows. The ODT velocity field is first set equal to $f(\widetilde{U}_i)_{k,i}$, a smooth continuous function whose cell average matches the initialized LES cell average values (see Eq. ()25) and Appendix A). The ODTLES evolution equations, without the advective terms, are then solved over a series of LES time steps. However, at the end of each time step the ODT velocity field is adjusted (as explained in Section 2.3.5) to be consistent with the original LES field. In this manner the ODT resolved substructure is built up while maintaining the same initial LES velocity field. As will be shown below, this method is only partially successful at introducing ODT resolved substructure into the initial state. As a result, the ODT resolved velocity spectrum is not well represented until later times in the calculations shown here.

3.2 Comparisons with the experimental data of Kang et al. [5]

3.2.1 Reference Calculations

Table 1 lists the key mesh and model parameters of the four reference calculations performed with ODTLES. These runs illustrate the impact of increasing the ODT-scale resolution while maintaining the same LES-scale mesh. All other parameters are held constant and equal to values determined from theoretical, heuristic or numerical considerations. In the next subsection, these other model parameters are varied to illustrate how sensitive the results are to these values.

Table 1. Key Parameters for the Reference Set of Calculations

Run	N_{les}	N_{odt}	N_{cell}	$L_{max}/\Delta X$	$\Delta T/\Delta T_{cfl}$	$C/\sqrt{54}$	C_{emc}
1	32	128	4	4	0.1	1.0	.002
2	32	256	8	4	0.1	1.0	.002
3	32	512	16	4	0.1	1.0	.002
4	32	1024	32	4	0.1	1.0	.002

Figure 5 shows the total LES and total ODT resolved kinetic energy as a function of time during all four reference calculations. In each case, the LES resolved energy is held constant during the ODT initialization period (from t=-0.75 to 0 sec.), but the ODT resolved energy grows until a plateau is reached. As can be clearly seen, higher values of N_{odt} allow a larger amount of the sub-grid kinetic energy to be resolved. At time t=0 sec, the turbulent flow is allowed to evolve according to the full set of equations and its energy rapidly decays. Although all four runs are quite similar, it can be seen that the LES-resolved energy decay for Run 1 is a little bit slower than for the others. This is because the smallest eddies are not being resolved when $N_{cell} = 4$. These unresolved eddy events, although not dominant, contribute a small amount to the dynamic inviscid process by which energy is transferred out of the LES resolved field.

Further insight into what is happening during the ODT initialization period can be gleaned from Fig. 6. Here we see a plot of the transverse one-dimensional energy spectra E_{22} at different times during the initialization period compared to the experimental data. Initially, the high-wave-number velocity spectra correspond to the 3D box-filtered values based on the smooth interpolating (or reconstruction) function $f(\widehat{\overline{U_i}})_{k,i}$. However, the energy in the high wave-numbers very quickly smooths out and begins to rise. The values plateau at about an order of magnitude lower than the data because they are being constrained to match the low-wave-number 3D LES spectrum.

The LES-resolved 3D energy spectrum from each reference run is compared to the experimental data in Fig. 7. Since the LES velocity field is initialized to spectrally match the X/M = 20 experimental data, all four cases follow data exactly out to the LES Nyquist limit at this point. At the later two times, the LES-resolved ODTLES results do not match the data exactly because the LES-resolved field is a spatially filtered quantity (similar to a box filter) that must quickly drop to zero as the Nyquist limit is passed. However, with this consideration taken into account, all four cases compare well with the data, and differences between them are very minor. This is another

indication that the eddy events are properly transferring energy from the low wave-numbers (resolved by the LES velocities) to the higher wave-numbers resolved only on the ODT domain. The slightly higher values seen for run 1 reflect the previously mentioned fact that the effects of the smallest eddy events are missing in this case (due to the coarse ODT mesh resolution).

The next four figures compare the transverse 1D energy spectra E_{22} from runs 1-4 with the data from the four experimental data stations. (Note that because the two ODT velocity components are normal to each line, the longitudinal 1D energy spectrun E_{11} cannot be directly computed.) In these figures the experimental data is plotted as well as two reference lines. The smaller vertical line corresponds to the wave-number of the wind tunnel height H. At wave-numbers approaching this value, and lower, the turbulence in the experiment is not isotropic, and thus the data is not valid for our comparison (see Kang et al. [5]) for details). The other vertical line shown corresponds to the LES Nyquist limit.

Figure 8 corresponds to the initialized state at time zero. Although the 3D spectrum is exactly matched at this point in time, for reasons described previously the 1D spectrum is not. Therefore a noticeable dip in the spectrum is seen at the LES Nyquist limit. In Figures 9 to 11 we see the 1D spectrum recover nicely as the flow evolves and energy from the low wave number regions cascades down into the high wave-numbers. By the third and fourth stations the 1D spectra from each run does a very good job of following the experimental data out to the limits of their respective resolutions.

In each of these runs energy is being dissipated by viscous effects at the highest resolved wave numbers. This is where the EMC model affects the problem, providing the amount of additional eddy viscosity needed to account for the eddies not being explicitly modeled. Note that although the EMC model constant C_{emc} is invariant, the eddy viscosity scales on the square of the cut-off length-scale l_{max} (see Eq. (20)). l_{max} is defined as the largest unresolved eddy event, which is just larger than the smallest resolved eddy event. Since the smallest eddy event that can be captured is equal to $6\Delta x$, we know that $l_{max} = L_{min} = 6\Delta x$. In the next sub-section, the effect of turning the EMC model off will be illustrated, as well as the sensitivity of the results to the value specified for C_{emc}.

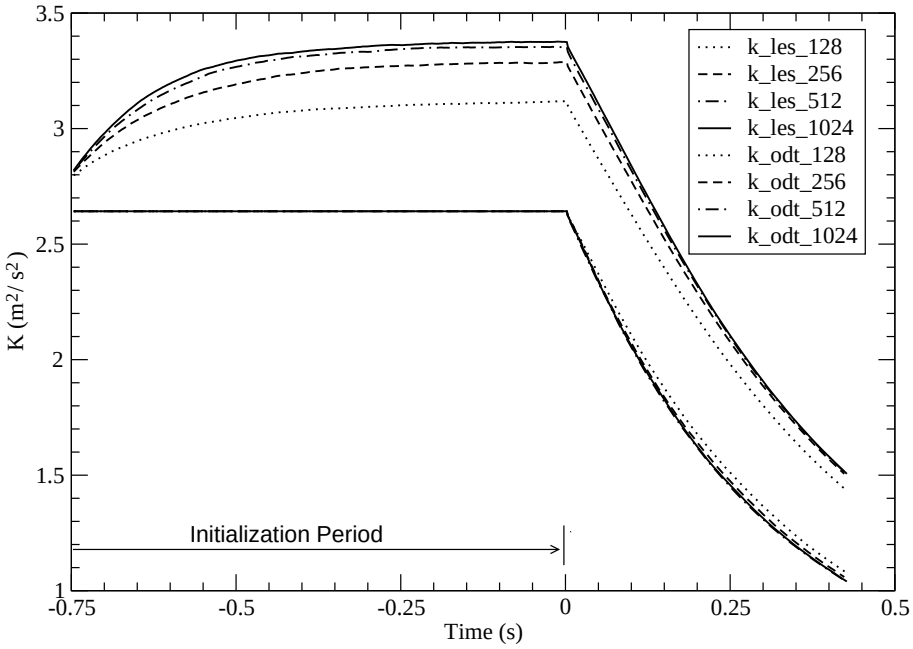

Figure 5. LES (lower curves) and ODT (upper curves) resolved kinetic energy as a function of time.

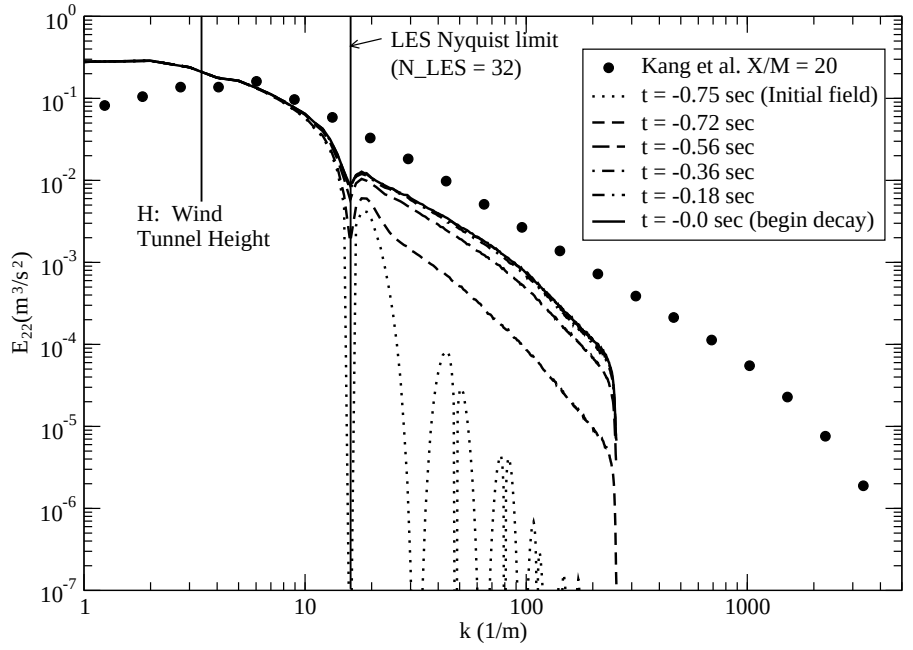

Figure 6. 1D energy spectra E_{22} during the initialization period.

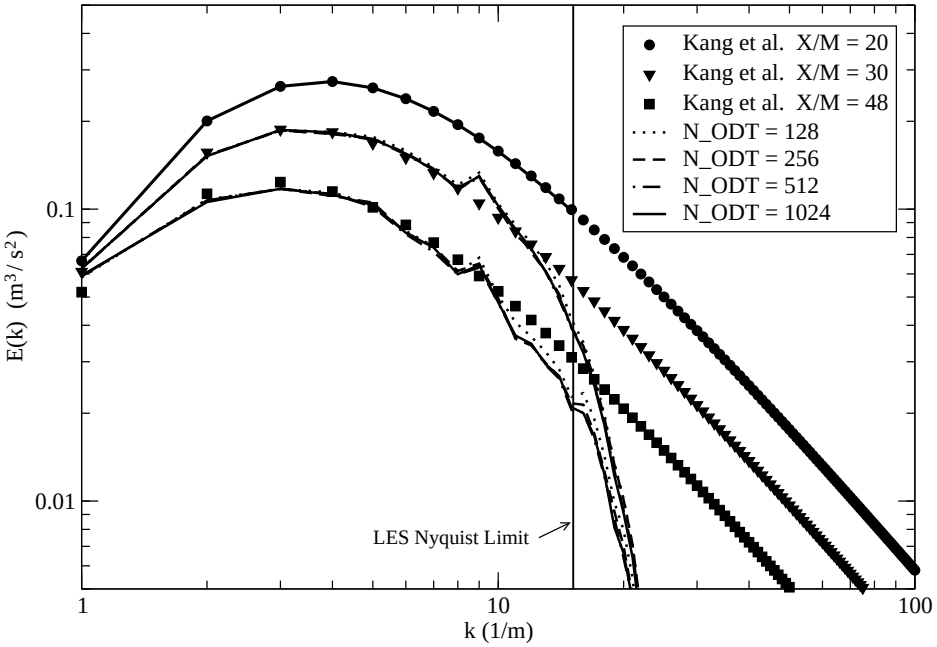

Figure 7. 3D energy spectra for each reference run.

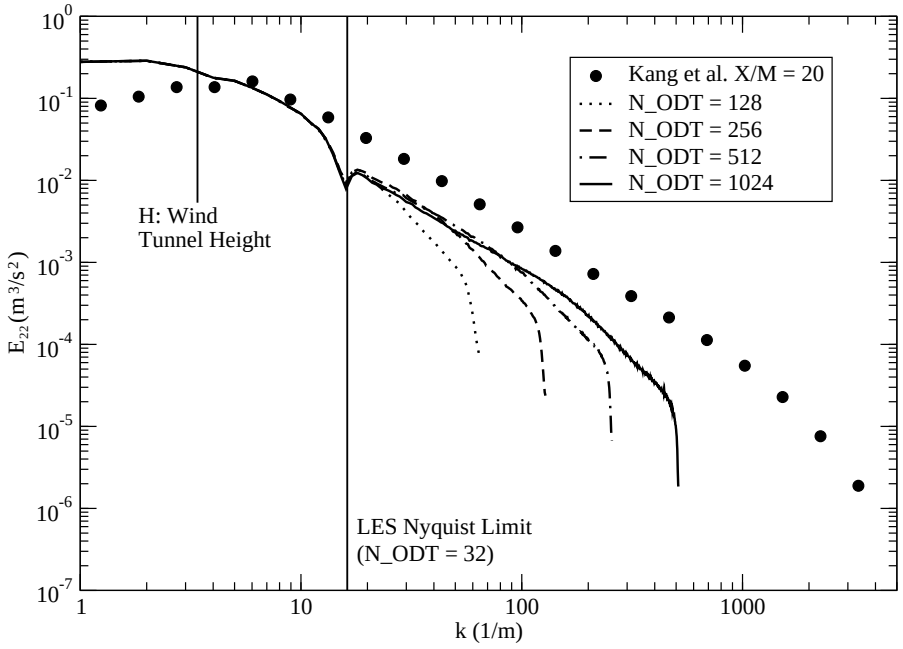

Figure 8. 1D energy spectra E_{22} at time t = 0 sec. for runs 1-4.

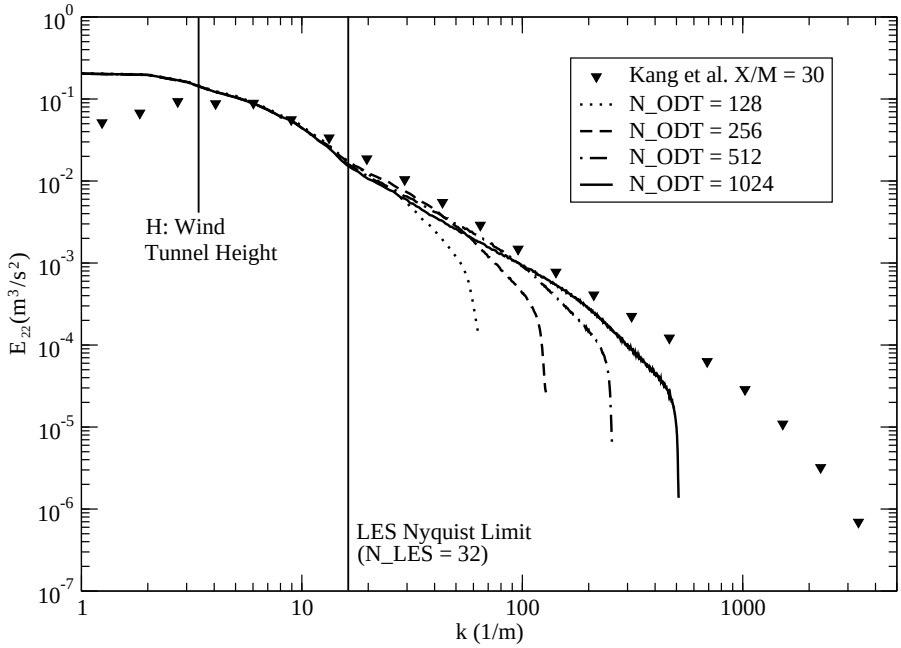

Figure 9. 1D energy spectra E_{22} at time t = 0.15 sec. for runs 1-4.

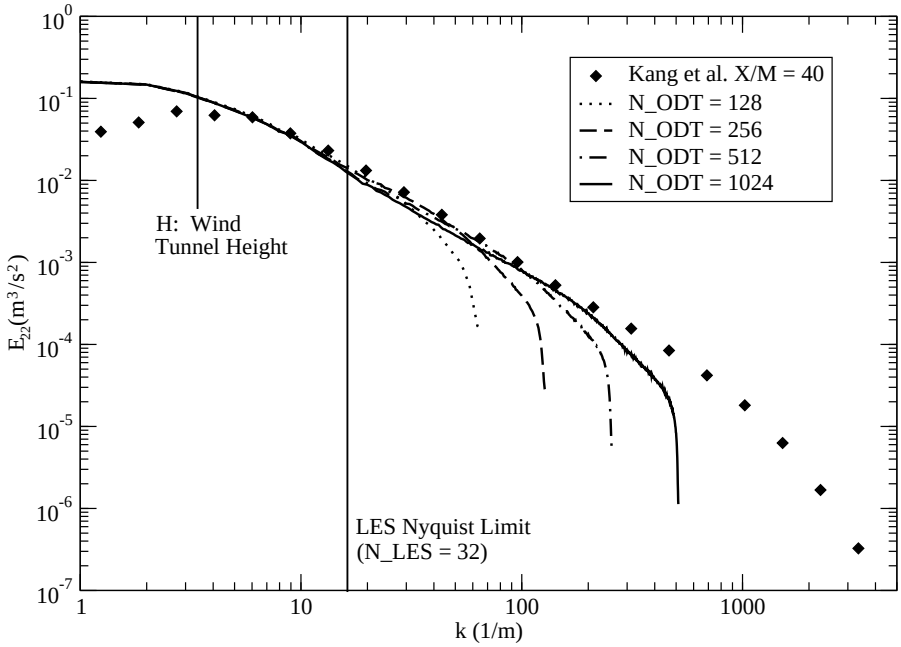

Figure 10. 1D energy spectra E_{22} at time t = 0.30 sec. for runs 1-4.

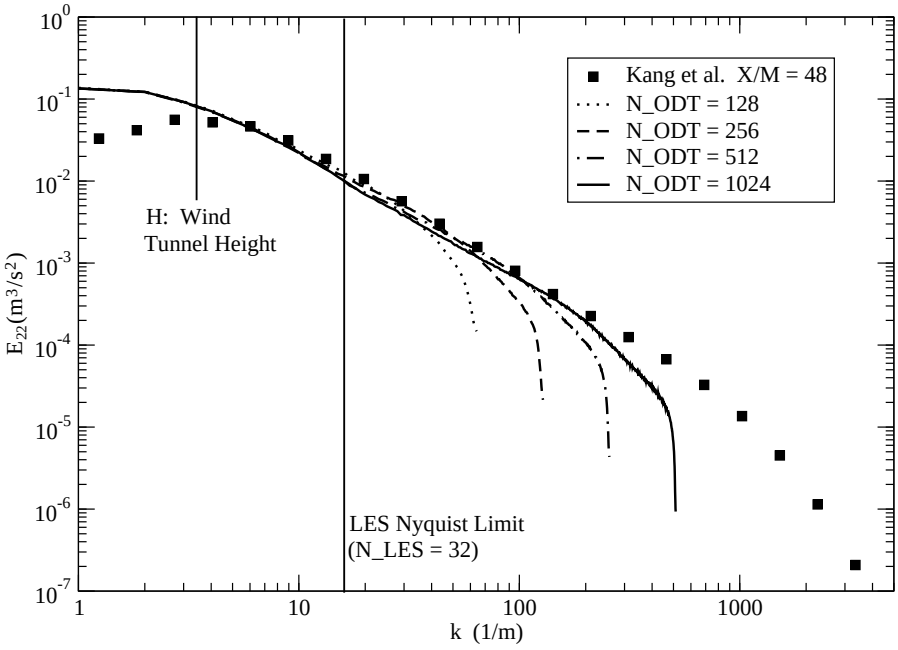

Figure 11. 1D energy spectra E_{22} at time t = 0.42 sec. for runs 1-4.

3.2.2 Sensitivity to Model parameters

A series of additional runs indicate the sensitivity of the results to mesh size and model parameters used in ODTLES. These runs are listed in Table 2.

Table 2. Calculations to Test Model Parameter Sensitivity

Run	N_{les}	N_{odt}	N_{cell}	$L_{max}/\Delta X$	$\Delta T/\Delta T_{cfl}$	$C/\sqrt{54}$	C_{emc}
5	64	256	4	4	0.1	1.0	.002
6	64	512	8	4	0.1	1.0	.002
7	32	256	8	3	0.1	1.0	.002
8	32	256	8	3	0.1	1.3	.002
9	32	256	8	6	0.1	1.0	.002
10	32	256	8	6	0.1	0.77	.002
11	32	128	4	4	0.2	1.0	.002
12	32	128	4	4	0.33	1.0	.002
13	32	256	8	4	0.1	1.0	0
14	32	256	8	4	0.1	1.0	.0025

Runs 5 and 6 essentially repeat runs 2 and 3, but with twice the LES resolution. All other code parameters are kept the same. In Figures 12 and 13 the 3D energy spectra and the 1D energy spectra are compared. As expected, the higher resolution is reflected in a larger portion of the 3D spectral energy being resolved on the LES grid. However, the 1D spectra at the last experimental data point (X/M=48) compare very closely. The only difference noted in Figure 13 is a slight suppression of the E_{22} spectra in the $N_{les} = 64$ runs in the region between the two Nyquist limits. The reason for this small artifact is unclear. Otherwise the curves appear to lie right on top of one another.

As has been more thoroughly discussed by McDermott [8], the values of L_{max} and C control the rate at which lower wave-number energy resolved by the LES mesh is transferred to the higher wave-number energy resolved only on the 1D grid. This cascade of energy is an inviscid process that, in ODTLES, is affected by both the overall rate at which eddy-events occur and the eddy-size distribution. Therefore, the energy decay rate itself does not uniquely determine the values of C and L_{max}. Although some interesting theoretical work [8] has been completed that provides certain constraints, the values chosen here are based primary on heuristic arguments and numerical experiments. The purpose of Runs 7-10 is to illustrate the sensitivity of the calculations to the value chosen for L_{max}, and how this choice affects the value of C that must be specified to obtain the correct decay rate.

From a conceptual standpoint, L_{max} should mark the length scale between the smallest real 3D eddies resolved on the 3D LES mesh, and those eddies that must be modeled by ODT eddy events. Since the ODTLES method is cast in a volume-balance context (that acts in physical space), spectral methods are not applicable and the value of L_{max} cannot be exactly specified from a numerical resolution standpoint. However, it seems reasonable to consider the Nyquist limit

($2\Delta X$) as a lower bound for L_{max}, and for practical purposes we would expect it to be at least $3\Delta X$. For the reference calculations discussed above, $L_{max} = 4$ was chosen. With this choice, it was found that the value of C which yielded the correct energy decay rate was $1.0/\sqrt{54}$, which agrees well with the theory developed in[8]. In Runs 7 through 10 we consider the effect of using $L_{max} = 3$ and $L_{max} = 6$.

The effect of changing L_{max} on the LES-resolved and ODT-resolved kinetic energy is shown in Figures 14 and 15. Several things can be noticed in looking carefully at these figures. First, decreasing L_{max} reduces both the ODT-resolved energy obtained during the initialization phase and the subsequent decay rate during the evolution phase. Conversely, increasing L_{max} increases both the ODT resolved energy obtained during the initialization phase and the subsequent decay rate during the evolution phase. To recover the same decay rate in the LES resolved energy, the ODT rate constant must also be adjusted. When L_{max} was reduced to $3\Delta X$, increasing C by 30 percent was required. When L_{max} was increased to 6 ΔX, C had to be lowered by 23 percent.

The trends described in reference to Figures 14 and 15 are also reflected in the results shown in Figures 16 and 17. These figures show the 3D energy spectra resolved on the LES mesh for runs 7-10, and compare them with run 2. Here we can note that the effect of these parameter variations is strongest in the higher wave-number regions. This is expected because this is the region where the larger-scale eddy events have an impact on the resolved 3D flow structures.

Figures 18 and 19 complete the story by showing the ODT resolved 1D spectra at experiment station X/M=48 for runs 7-10, and compare them with run 2. Although the effect is small, different combinations of L_{max} and C are seen to yield slightly different slopes. This may be useful in further refining what the most appropriate values of L_{max} and C should be.

Runs 11 and 12 were made to verify that the LES time step taken during the reference runs was small enough. These runs confirmed that the time step was sufficiently small because results for both these runs were statistically identical in all key aspects to reference run 1. For this reason, no plots are shown concerning these runs.

Runs 13 and 14 explore the impact of the EMC model and its associated constant, C_{emc}.

In Run 13, the EMC model was turned off. This resulted in a large energy buildup in the high-wave-number region because the ODT resolution was not sufficient to dissipate the energy at the proper scales. This is reflected in Figure 20, where the 1D energy spectra at two times in the calculation are plotted for runs with and without the EMC model active. As can be seen, the effect is dramatic and totally distorts the solution.

In Figure 21 we compare the 1D energy spectra at the end of the simulation time period for two different values of the EMC model constant, $C_{emc} = .0020$ (the reference value), and $C_{emc} = .0025$. Results show that only the energy at the highest wave-numbers is affected by this change. Although the difference is small, the slope obtained using the higher value appears to be more consistent with the experimental data shown, suggesting that perhaps the higher value is a better choice.

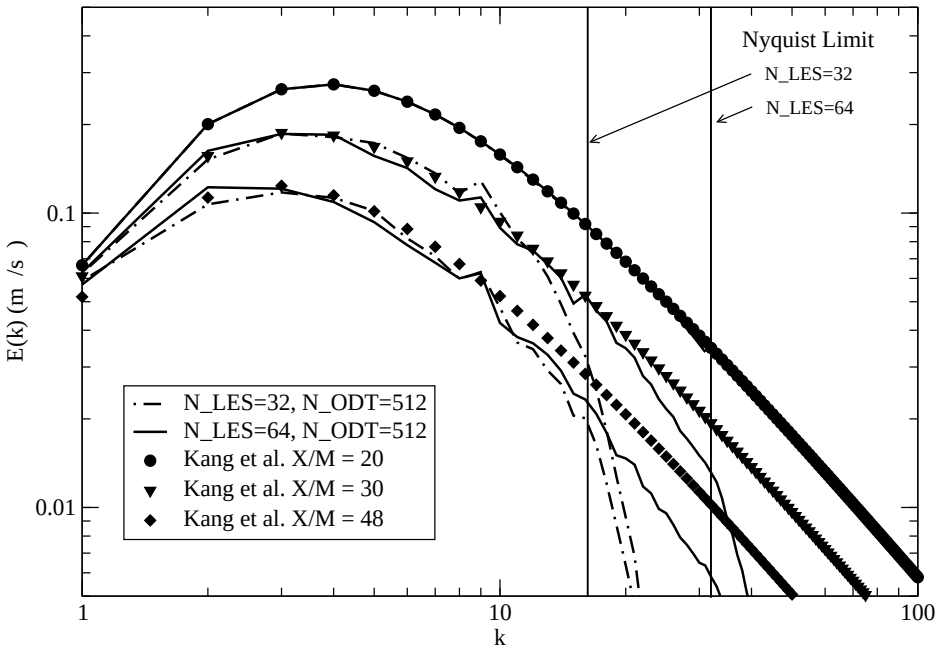

Figure 12. Effect LES mesh resolution on 3D energy spectra.

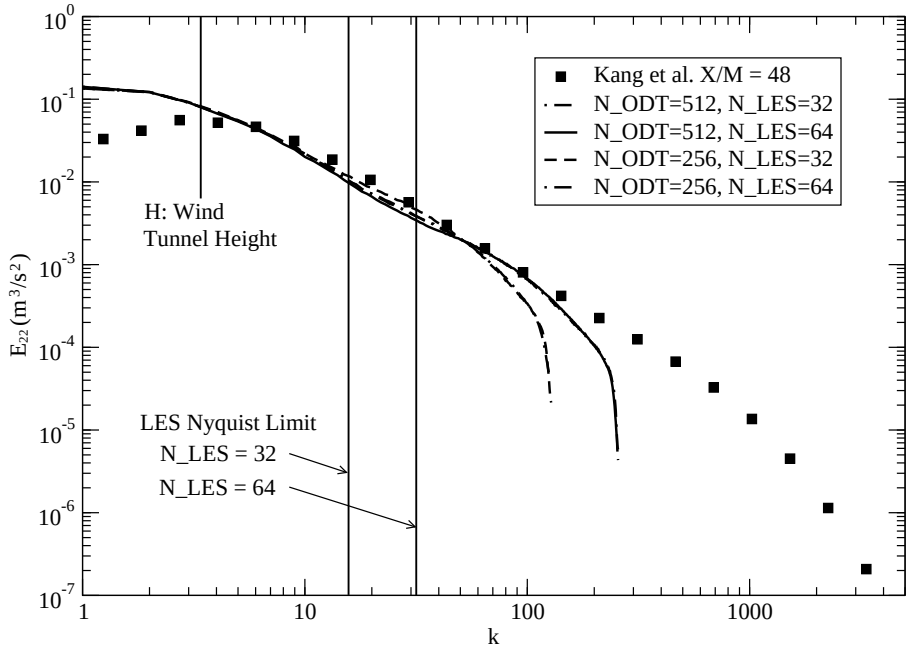

Figure 13. Effect LES mesh resolution on 1D energy spectra E_{22}.

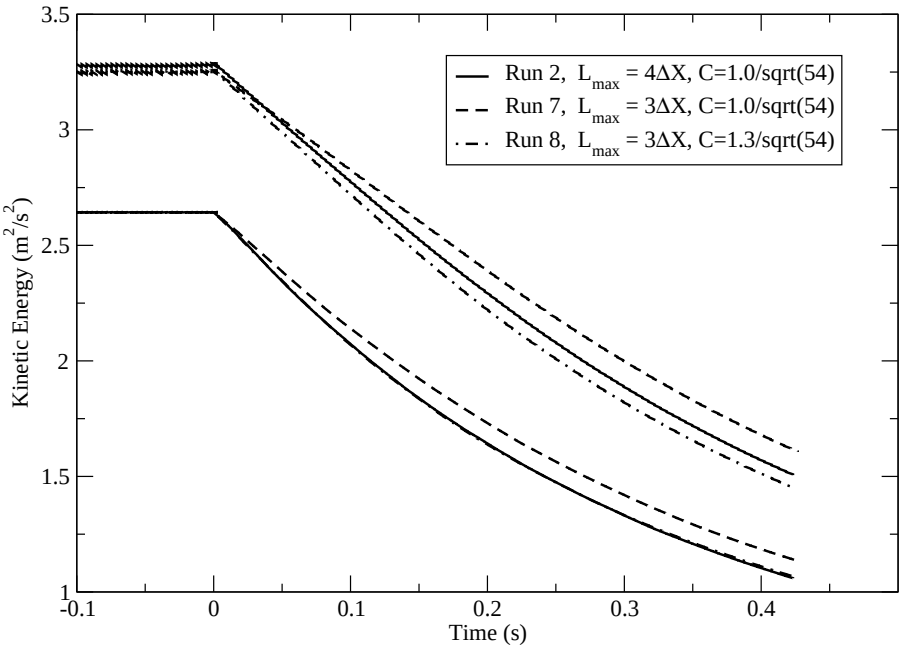

Figure 14. Sensitivity of LES (lower curves) and ODT (higher curves) resolved kinetic energy decay to reducing L_{max}.

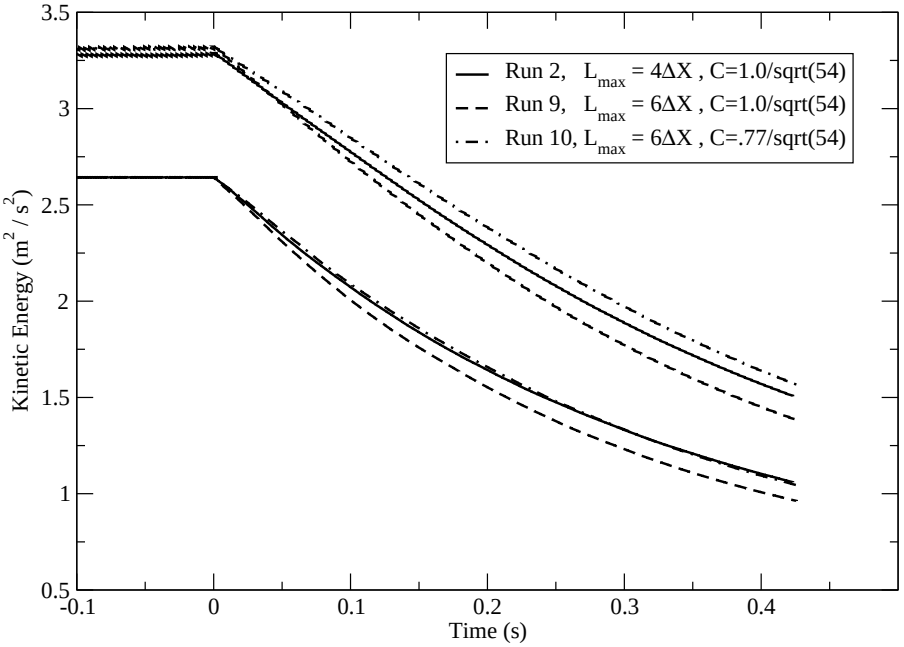

Figure 15. Sensitivity of LES (lower curves) and ODT (higher curves) resolved kinetic energy decay to increasing L_{max}.

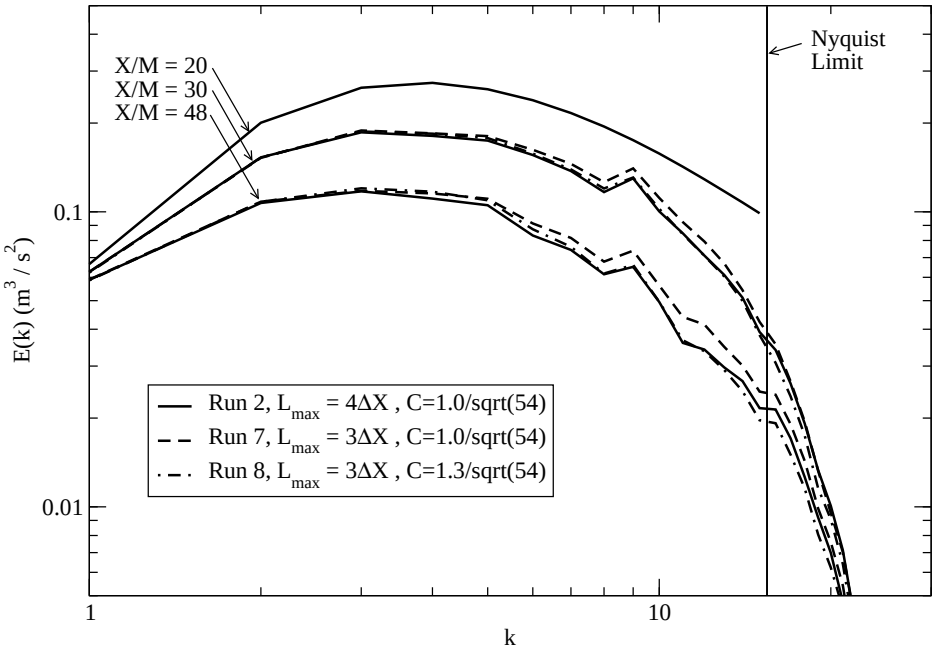

Figure 16. Sensitivity of the 3D energy spectra to reducing L_{max}.

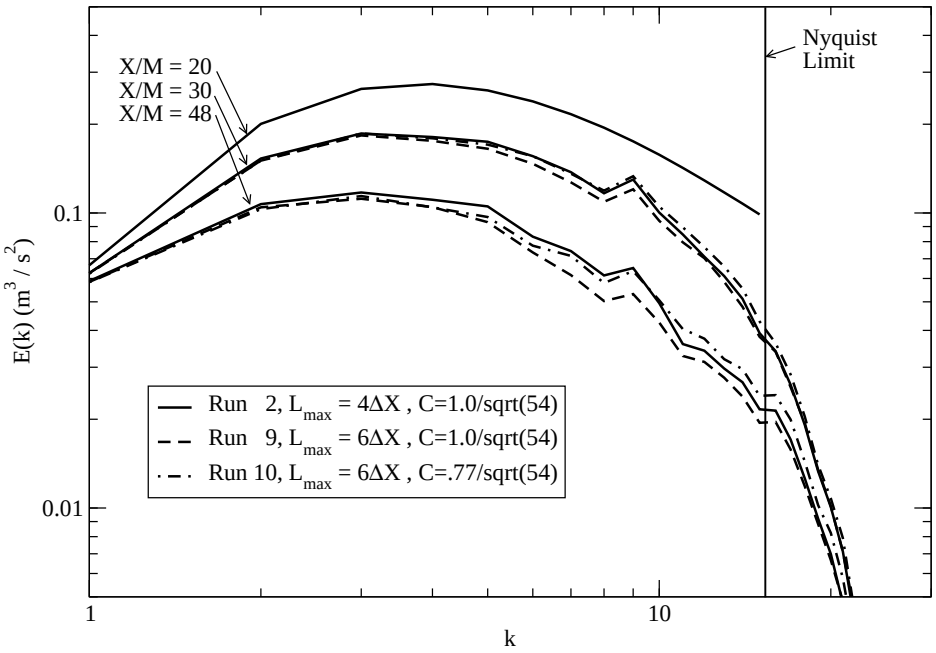

Figure 17. Sensitivity of the 3D energy spectra to increasing L_{max}.

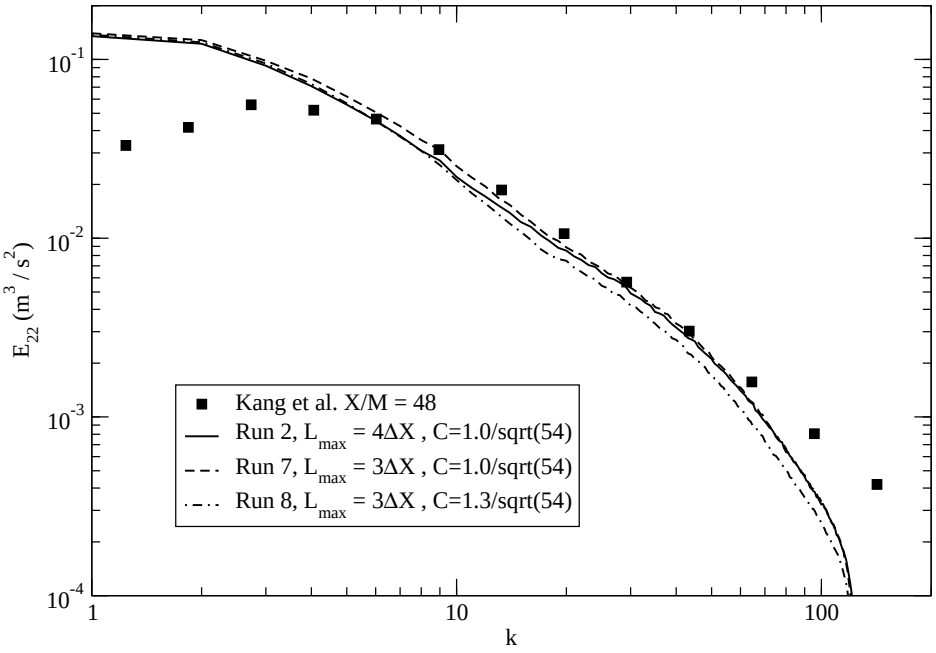

Figure 18. Sensitivity of the 1D energy spectra to reducing L_{max}.

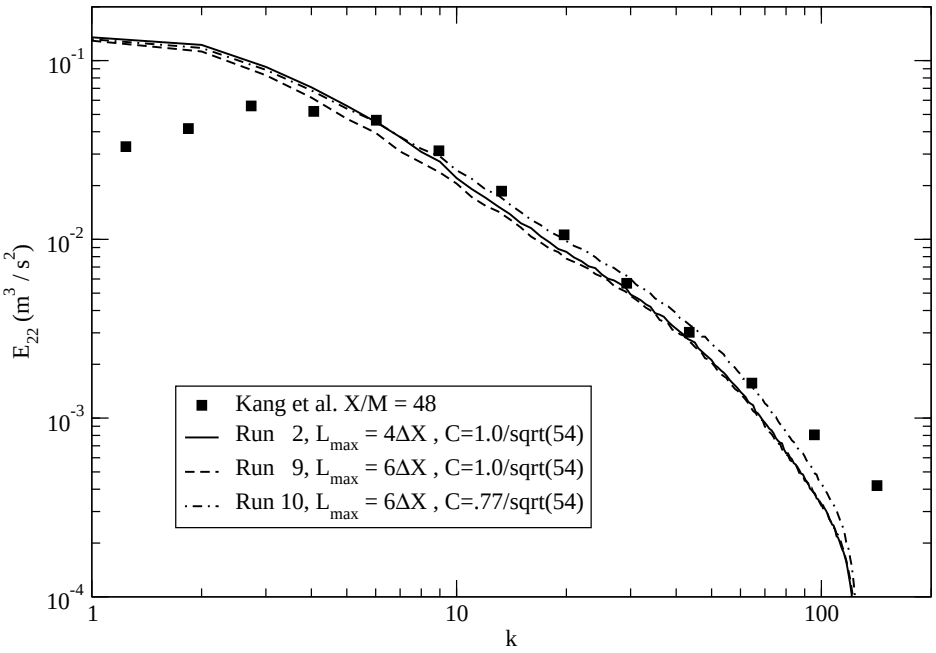

Figure 19. Sensitivity of the 3D energy spectra to increasing L_{max}.

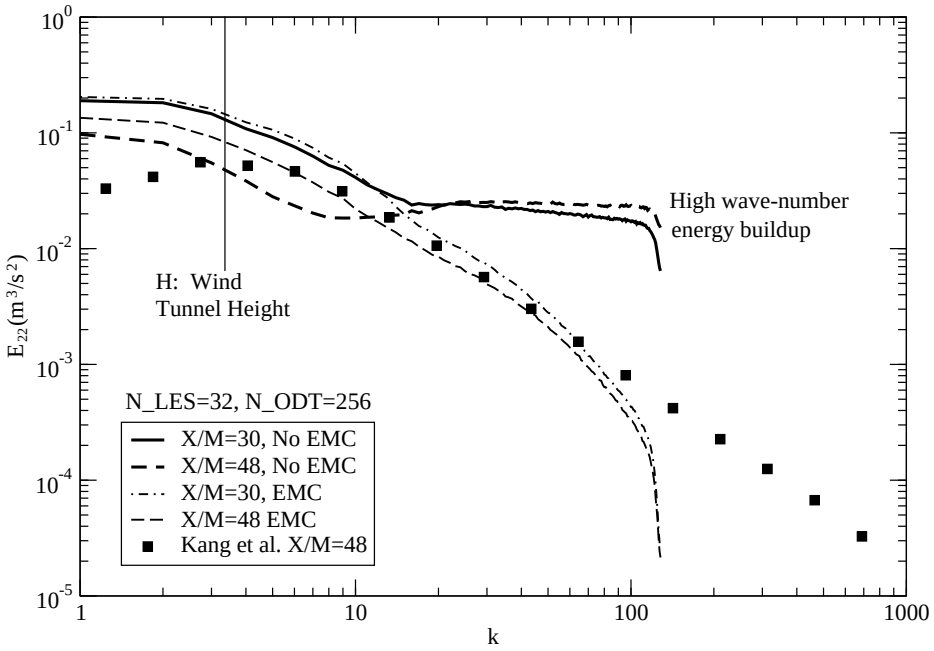

Figure 20. The effect on the 1D energy spectra of turning the EMC model off.

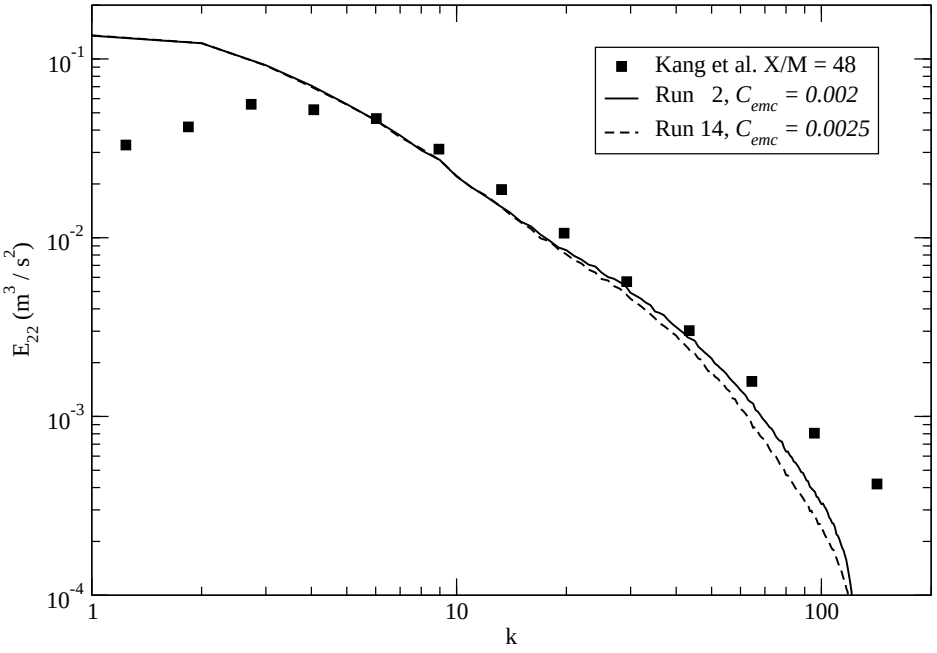

Figure 21. Sensitivity of the 1D energy spectra to increasing C_{emc}.

References

[1] W. T. Ashurst and A. R. Kerstein. One-dimensional turbulence: Variable-density formulation and application to mixing layers. *Phys. Fluids. in press*, 2005.

[2] S. Cant. High-performance computing in computational fluid dynamics: progress and challenges. *Phil. Trans. Royal Society of London Series A - Math. Phy. Eng. Sci.*, 360:1211–1225, 2002.

[3] G. Comte-Bellot and S. Corrsin. Simple Eulerian correlation of full-and narrow band velocity signals in grid-generated 'isotropic' turbulence. *Journal of Fluid Mechanics*, 48:273–337, 1971.

[4] J. W. Deardorff. The use of subgrid transport equations in a three-dimensional model of atmospheric turbulence. *ASME J. Fluids Engng.*, page 429, 1973.

[5] H. Kang, S. Chester, and C. Meneveau. Decaying turbulence in an active-grid-generated flow and comparisons with large-eddy simulations. *J. Fluid Mech.*, 480:129, 2003.

[6] A. R. Kerstein. One-dimensional turbulence: Model formulation and application to homogeneous turbulence, shear flows, and buoyant stratified flows. *J. Fluid Mech.*, 392:277, 1999.

[7] A. R. Kerstein, W. T. Ashurst, S. Wunsch, and V. Nilsen. One-dimensional turbulence: Vector formulation and application to free shear flows. *J. Fluid Mech.*, 447:85, 2001.

[8] R. J. McDermott, A. R. Kerstein, R. C. Schmidt, and P. J. Smith. Ensemble mean closure based on one-dimensional turbulence. *in preparation*, 2005.

[9] S. B. Pope. *Turbulent Flows*. Cambridge University Press, 2000.

[10] P. Sagaut. *Large Eddy Simulation for Incompressible Flows*. Springer-Verlag, 2001.

[11] R. Schmidt, A. Kerstein, S. Wunsch, and V. Nilsen. Near-wall LES closure based on one-dimensional turbulence modeling. *J. Comput. Phys.*, 186:317, 2003.

[12] R. C. Schmidt, T. M. Smith, P. E. Desjardin, T. E. Voth, M. A. Christon, A. R. Kerstein, and S. Wunsch. On the development of the large eddy simulation approach for modeling turbulent flow: LDRD Final Report. Report No. SAND2002-0807, Sandia National Laboratories, 2002.

[13] U. Schumann. Subgrid scale model for finite difference simulation of turbulent flows in plane channels and annuli. *J. Comput. Phys.*, 18:376, 1975.

[14] S. Völker, R. D. Moser, and P. Venugopal. Optimal large eddy simulation of turbulent channel flow based on direct numerical simulation statistical data. *Physics of Fluids*, 14:3675, 2002.

A An efficient discrete reconstruction procedure that preserves cell averages

Consider a 1D function $f(x)$, whose box-filtered values

$$\overline{U}(x_j) = \frac{1}{h}\int_{x_j-h/2}^{x_j+h/2} f(x)dx \tag{39}$$

are known at N uniformly spaced locations x_j, on a domain $0 < x < L$, where $h = L/N = (x_{j+1} - x_j)$, and whose boundary conditions, $f(0)$ and $f(L)$ are known.

We desire to find a well-behaved, smooth set of M ($M = KN$, where $K = 2^n$) values of $\overline{u}(x_i)$, at uniformly spaced locations x_i, that exactly satisfy the relationship

$$\overline{U}(x_j) = \frac{1}{K}\sum_{i=(j-1)K}^{jK} \overline{u}(x_i). \tag{40}$$

and which are consistent with the known boundary conditions.

The algorithm described here computes a set of 2N values of $\overline{u}(x_i)$ from the initial set of N values of $\overline{U}(x_j)$. The process can be repeated (n-1) more times to obtain the desired refinement corresponding to any value of K.

To help understand the algorithm we refer the reader to Figure A.1, which illustrates a simple case where N=3, and the function $f(x)$ is assumed periodic. The values of $\overline{U}_j(x_j)$, j=1,3 are respectively, 4, 6, and 1.

Values of $\overline{u}(x_i)$ are found through an iterative process that, by construction, always enforces Eq. (40). Each iteration step, a set of 2N "starred" values, $\overline{u}^*(x_i)$, are computed as

$$\overline{u}^*(x_{i-}) = \frac{\overline{U}(x_j) + f^*(x_j - h/2)}{2} \tag{41}$$

$$\overline{u}^*(x_{i+}) = \frac{\overline{U}(x_j) + f^*(x_j + h/2)}{2} \tag{42}$$

where $i-$ and $i+$ denote, respectively, the first and second values of i located in cell j, and f^* denotes a current iteration estimate of the interpolated value for $\overline{u}$ at the cell boundaries. These are estimated in a manner to be explained next, except if the cell boundary corresponds to one of the domain boundaries, $x = 0, L$, and the boundary conditions for $f(x)$ are specified. In this case, we simply set $f^*(0) = f(0)$, and $f^*(L) = f(L)$.

On the first iteration, the values of $f^*(x_j - h/2)$ and $f^*(x_j + h/2)$ are computed as a linear interpolation at the midway points between the $\overline{U}(x_j)$, i.e.

$$f^*(x_j - h/2) = \frac{\overline{U}(x_j) + \overline{U}(x_{j-1})}{2} \tag{43}$$

$$f^*(x_j + h/2) = \frac{\overline{U}(x_j) + \overline{U}(x_{j+1})}{2} \tag{44}$$

At each succeeding iteration, they are computed by interpolation between past iterate values of $\overline{u}(x_i)$ as follows:

$$f^*(x_j - h/2) = \frac{\overline{u}(x_{i-}) + \overline{u}(x_{i--})}{2} \tag{45}$$

$$f^*(x_j + h/2) = \frac{\overline{u}(x_{i+}) + \overline{u}(x_{i++})}{2} \tag{46}$$

Here, *i*++ denotes the value of (*i*+)+1, and *i*– denotes the value of (*i*-)-1.

No matter how the values of $f^*(x_j - h/2)$ and $f^*(x_j + h/2)$ are computed, the next iterate values of $\overline{u}(x_i)$ are always calculated by adding a correction C_j to the starred values, $\overline{u}^*(x_i)$, as follows.

$$\overline{u}(x_{i-}) = \overline{u}^*(x_{i-}) + C_j \tag{47}$$

$$\overline{u}(x_{i+}) = \overline{u}^*(x_{i+}) + C_j \tag{48}$$

where

$$C_j = \overline{U}_j(x_j - \frac{\overline{u}(x_{i-}) + \overline{u}(x_{i+})}{2} \tag{49}$$

Note that the value of C_j is calculated so that, by construction, Eq. (40) is identically satisfied.

The method converges rapidly as the iterations proceed. Experience using this method in the context of ODTLES suggests that four iterations are sufficient for all practical purposes.

In the limit of large M, the method produces a smooth continuous approximation of the function $f(x)$ that exactly satisfies the Eq. (39). Other approximations can be generated using alternative schemes and, in fact, an infinite number of solutions exist. However, this method is computationally fast, stable, and well behaved. Figure A.2 shows results from performing the reconstruction procedure for a case where N = 16, M = 256, and the domain is periodic.

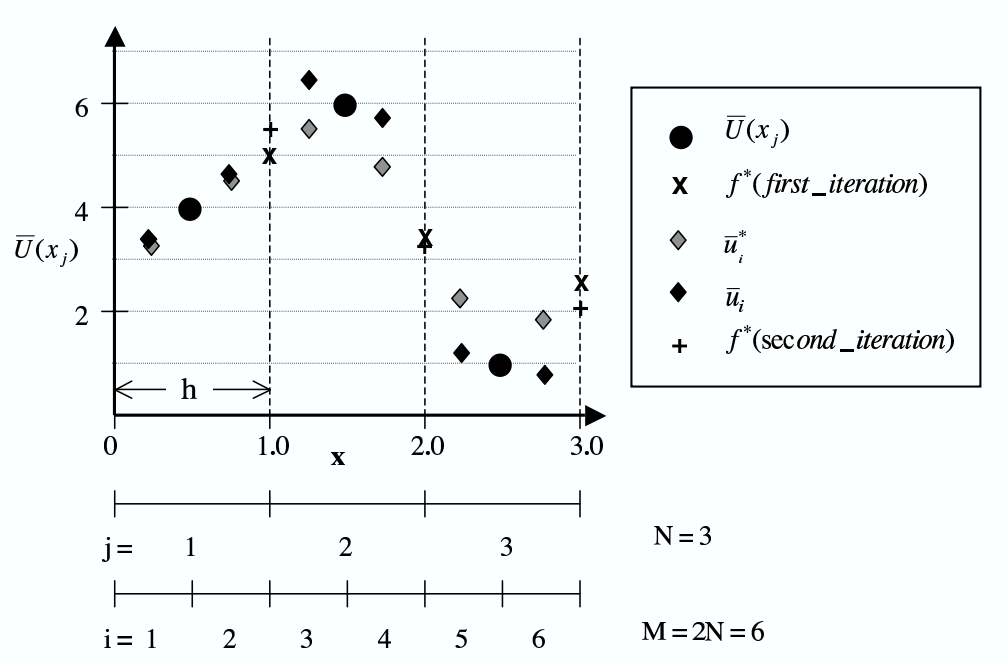

Figure A.1. Simple illustration of initial steps in the discrete reconstruction procedure.

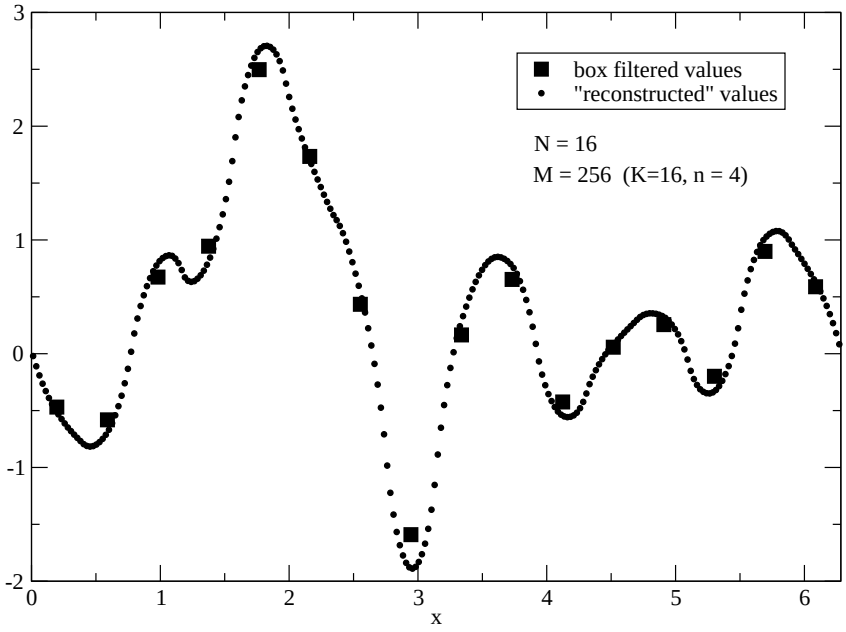

Figure A.2. Example discrete reconstruction for N = 16, M = 256.

DISTRIBUTION:

2 Randy McDermott
University of Utah, INSCC
155 S. 1452 E., Rm 380
Salt Lake City, UT 84112

5 MS 0316
Rodney C. Schmidt, 9233

1 MS 0316
John Shadid, 9233

1 MS 0316
Tom Smith, 9233

1 MS 0316
Sudip Dosanjh, 9233

1 MS 0378
Mark Christon, 9231

1 MS 0370
Tim Trucano, 9211

1 MS 0384
Carl Peterson, 9100

1 MS 0382
Stefan Domino, 9141

1 MS 1135
Sheldon Tieszen, 9132

1 MS 0825
Fred Blottner, 9115

5 MS 9051
Alan Kerstein, 8351

1 MS 9409
Chris Moen, 8775

1 MS 0742
Dana Powers, 6870

1 MS 0665
Scott Wunsch, 2542

1 MS 0123
LDRD office (Donna L. Chavez), 01011

1 MS 9018
Central Technical Files, 8940-2

2 MS 0899
Technical Library, 4916